Synergy between metals for small molecule activation: Enzymes and bio-inspired complexes

Ashta Ghosh, Carole Duboc, Marcello Gennari

Synergy between metals for small molecule activation: enzymes and bio-inspired complexes

Ashta C. Ghosh[a,b], Carole Duboc[a], Marcello Gennari[a]*

[a] *Univ. Grenoble Alpes, UMR CNRS 5250, Département de Chimie Moléculaire, 38000 Grenoble, France*
[b] *Univ. Lyon, Université Claude Bernard Lyon 1, CNRS, IRCELYON - UMR 5256, 2 Avenue Albert Einstein, 69626 Villeurbanne Cedex, France*

* corresponding author: marcello.gennari@univ-grenoble-alpes.fr

Keywords

homogeneous multimetallic redox catalysts
metal-metal cooperation
small molecule activation
bio-inspired chemistry
reaction mechanism
metalloenzymes

Abstract

Transition metal-driven small molecule activation is essential for the production of fuels and chemicals or energy supply. The use of multimetallic catalysts, where two or more metal centers act in synergy to activate and transform the substrate(s), is widespread both in nature (metalloenzymes) and (bio)inorganic chemistry. Benefits of this strategy in terms of catalytic performances result from cooperation between different metals (i) to bind and activate a single substrate, (ii) to activate different substrates reacting together (typically one per metal), or (iii) with one "assisting" metal tuning the reactivity of the "active" metal center.

In this review, we discuss multimetallic active sites of enzymes and multimetallic synthetic bio-inspired complexes, for which the cooperation between metal centers is critical for the activation of small molecules. The following processes are considered: (i) H_2 production(/oxidation) ([FeFe]- and [NiFe]-hydrogenases); (ii) O_2 reduction (cytochrome *c* oxidase); (iii) CO_2 reduction and formation of C-C bonds (NiFe- and MoCu-dependent CO dehydrogenases and acetyl-CoA synthase); (iv) N_2 reduction (Mo-dependent nitrogenase); and (v) N_2O reduction (N_2O reductase). This overview is expected to contribute to understand the role of metal-metal synergy in enzymes and model complexes and its impact on reactivity. This

background, in combination with ligand design, can be exploited for the development of the next generation of bio-inspired multinuclear catalysts with optimized performances.

Contents

1. Introduction

Activation and catalytic conversion of small earth-abundant molecules by multielectron redox reactions are crucial for the production of fuels (e.g. H_2 from water) or useful chemicals (e.g. NH_3 or H_2O_2 by reduction of N_2 or O_2, formation of C-C bonds), for energy conversion (e.g. $4H^+/4e^-$ O_2 reduction), or for the removal of toxic gases from the atmosphere (e.g. reduction of CO_2 or N_2O) [1-6]. The most commonly adopted strategy is based on the use of transition metal-containing catalysts to overcome the kinetic issues of such reactions and to properly control their selectivity, when relevant [1-6]. This approach has been first adopted by nature with metalloenzymes then followed by bioinorganic chemists who attempt to model their active sites for the development of synthetic catalysts. Among such biological and bio-inspired systems, many contain multiple metal centers, which act in synergy to activate and transform the substrate(s). Two or more metal ions are kept in close proximity through bridging ligands (mostly thiolates or sulfides in nature), and/or constrained by the protein backbone or ligand scaffold (when using multitopic ligands). A direct metal-metal interaction can be also present

when low oxidation states are involved [7]. The multimetallic strategy can bring a significant benefit in terms of reactivity with respect to the use of single metal centers [8, 9], because: (i) two or more metals can interact with a substrate, sequentially or in a concerted way, to promote its activation; (ii) each metal can activate a different substrate before they react together; (iii) a larger number of electrons (or electron-holes) can be more easily stored, which is highly desirable for multielectron processes; (iv) one "assisting" metal can modulate the geometric, electronic and redox properties of the "active" metal to promote substrate binding, redox activation and/or to control proton/electron delivery.

This review focuses on biological and synthetic homo- and heterometallic complexes for small molecule activation, with particular emphasis put on the role of metal-metal cooperation for reactivity. Several enzymatic processes are described beginning with an overview of the structural properties of the active site of the targeted enzyme followed by a discussion on the reaction mechanism. Then, selected examples of structural and/or functional bio-inspired complexes are described. This review mostly focuses on reduction reactions, even if not exclusively; more specifically, the following processes are discussed: (i) H_2 production(/oxidation) ([FeFe]- and [NiFe]-hydrogenases); (ii) O_2 reduction (cytochrome *c* oxidase); (iii) CO_2 reduction and formation of C-C bonds (NiFe- and MoCu-dependent CO dehydrogenases and acetyl-CoA synthase); (iv) N_2 reduction (Mo-dependent nitrogenase); and (v) N_2O reduction (N_2O reductase). Since only selected examples of small molecules and of relevant synthetic models are considered, the present review is not exhaustive. The reader is invited to refer to the review articles cited in each specific section to access comprehensive lists. Whereas a few reviews have been published in recent years on multimetallic catalysts (mostly containing metal-metal bond(s)) for both organic and organometallic reactions [7-9], to our knowledge none have been dedicated to multimetallic synergy in enzymes and their synthetic models for application in the domain of energy conversion.

2. Hydrogen evolution (and oxidation): the example of [FeFe]- and [NiFe]-hydrogenases

The development of alternative energy production schemes represents a major challenge faced by our societies with the ever-increasing energy demand and climate change. Molecular hydrogen (H_2) is considered as a clean and promising medium to store energy that can be later released by oxidising it either via direct combustion or in fuel cells, without producing greenhouse gases [2, 10]. A ~95% of the available H_2 is currently produced from fossil fuels,

while water electrolysis is still not adapted for large scale H_2 production due to the need of expensive platinum catalysts. In nature, [FeFe]- and [NiFe]-hydrogenases (H_2ases) interconvert protons and electrons with dihydrogen (Eq. 1) in a highly efficient and clean way, through their thiolate-bridged {$MFeS_2$} catalytic centers (M = Fe or Ni) [11, 12].

$$2H^+ + 2e^- \leftrightarrows H_2 \qquad (1)$$

In both enzymes, two metal centers play in synergy to promote multiple proton and electron transfer events. Commonly, [FeFe]-H_2ases are more active for H_2 production (Hydrogen Evolution Reaction or HER) and [NiFe]-H_2ases for H_2 oxidation (Hydrogen Oxidation Reaction or HOR). Unfortunately, H_2ases are in general highly sensitive to dioxygen (with a few exceptions among the [NiFe]-H_2ases), limiting their incorporation into technological devices for widespread applications. Hence, intense research is devoted to the development of small molecule analogues of [NiFe]- and [FeFe]-H_2ase active sites as HER (or HOR) catalysts that will ideally replace platinum in water electrolysis cells (or hydrogen fuel cells) [13-19].

[FeFe]-H_2ases are composed of a single or multiple subunits with an essential core, named H-cluster, whose structure is well conserved within this family of enzymes [20]. The H-cluster is in close proximity of a network of iron-sulfur clusters, part of an electron transport (ET) chain. The H-cluster consists of a diiron [2Fe] and a [Fe_4S_4] subclusters connected via a thiolate from a cysteine residue [21, 22] (Fig. 1). The [2Fe] subcluster corresponds to the {$FeFeS_2$} catalytic unit, composed of two iron atoms bridged by an aza-propane-1,3-dithiolate (adt) ligand [12, 23] and a (semi-)bridged carbon monoxide [24, 25]. Each iron center of [2Fe] is further bound to one cyanide and one carbon monoxide co-ligands, all in a terminal coordination mode [26, 27]. While the iron atom "proximal" to the [Fe_4S_4] cluster (Fe_p) is coordinatively saturated, the "distal" iron (Fe_d) has an open coordination site, where the substrates (H_2 or H^+) bind. The secondary amine of the azadithiolate ligand plays a key role in shuttling H^+ to or from the active site and in promoting low energy transition states by virtue of its acid−base properties [20, 28, 29].

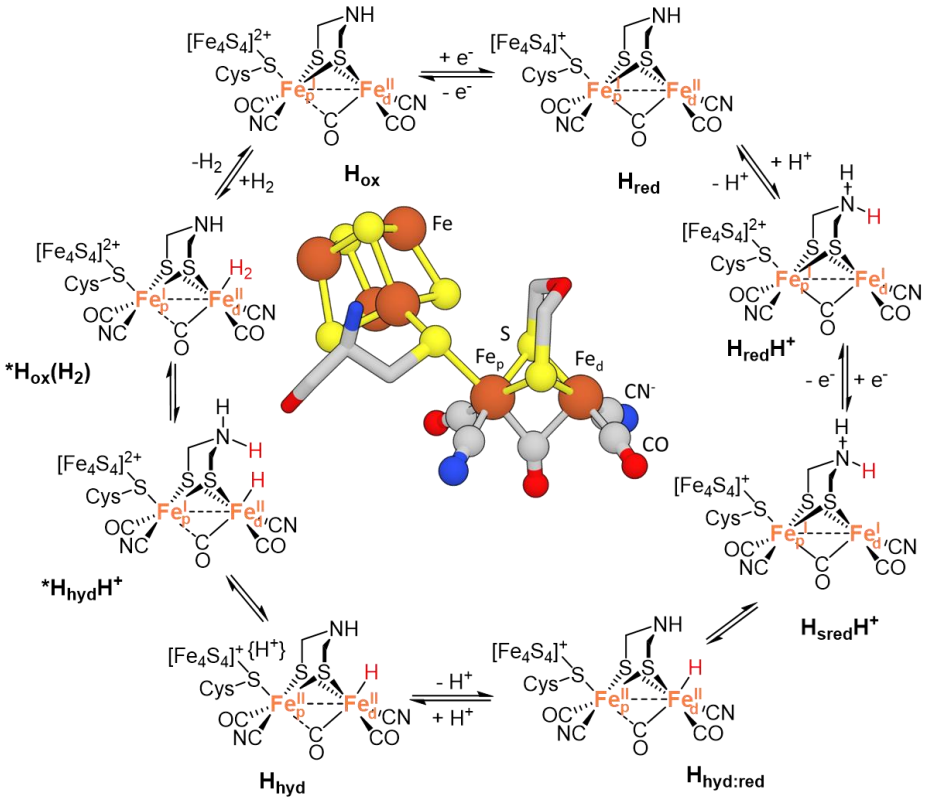

Fig. 1. Structure of the [FeFe]-H_2ase active site (PDB 3C8Y) and currently accepted catalytic cycle.

Even if several redox and protonation states of the H-cluster have been generated and characterized under different experimental conditions and from various bacteria, the reaction mechanism for H_2 production is still under discussion: are they all involved in the catalytic cycle? Is the mechanism common for all bacterial [FeFe]-H_2ases [20, 30]? Fig. 1 proposes a cycle mostly including species that have been isolated and proven to be active (H_{ox}, H_{red}, $H_{red}H^+$, $H_{sred}H^+$, $H_{hyd:red}$, H_{hyd}, in addition to $*H_{hyd}H^+$ and $*H_{ox}(H_2)$ that are only postulated). The first step corresponds to the reduction of the resting state (H_{ox}, $[Fe_4S_4]^{2+}$-$Fe_p^{I}Fe_d^{II}$) to generate the $[Fe_4S_4]^{+}$-$Fe_p^{I}Fe_d^{II}$ state (H_{red}) that binds the first proton at the bridgehead adt-N to form $H_{red}H^+$ [31-33]. Successive reduction and protonation result in a $[Fe_4S_4]^{+}$-$Fe_p^{II}Fe_d^{II}$–H{H^+} species (H_{hyd}), containing a hydride ligand terminally-bound to Fe_d [27, 34, 35]. The terminal hydride and the additional proton (whose localization is still not definitively clarified) then combine to produce H_2. This last step is certainly facilitated by proton transfer via the adt ligand prior of the generation of a Fe-H_2 adduct ($*H_{ox}(H_2)$). Each step is reversible, since H_2 oxidation is proposed to occur through the same catalytic steps, but in the opposite direction. While both Fe are implicated in the redox chemistry cycling between the +I and +II oxidation states, the Fe_d center is more directly implicated in substrate activation through the generation of the hydride

intermediate, H_{hyd}. The [4Fe4S] cluster acts as an electron reservoir during catalysis, cycling between the +1 and +2 states.

The synergy between Fe_d and Fe_p is crucial for the hydrogen evolution and oxidation reactions. This synergy is structurally and electronically mediated through the adt and CO bridging ligands [24], as well as a direct metal-metal interaction (Fe-Fe bond distance of 2.53 Å in the resting state) [36]. Fe_p is not only directly involved in redox activity but also serves (i) to position the amine function of the adt ligand close to Fe_d, in order to facilitate the relay of protons to or from it [12]; (ii) to stabilize, via the semi-bridging CO, Fe_d in an 'inverted' square pyramidal conformation that promotes substrate binding next to the amine proton relay; (iii) to foster electron delocalization/transfer between the $[Fe_4S_4]$ cluster and Fe_d for optimal efficiency during catalysis.

The [NiFe]-H_2ases are generally composed of two subunits, one lodging the heterobimetallic $\{NiFeS_2\}$ active site and one hosting three aligned iron-sulfur clusters responsible for the electron transport between a redox protein partner and the catalytic center [37]. The NiFe complex is composed of a $\{Ni(cysteinate)_4\}$ unit linked via two of its cysteine ligands to an $\{Fe^{II}(CN)_2(CO)\}$ moiety [38] (Fig. 2a).

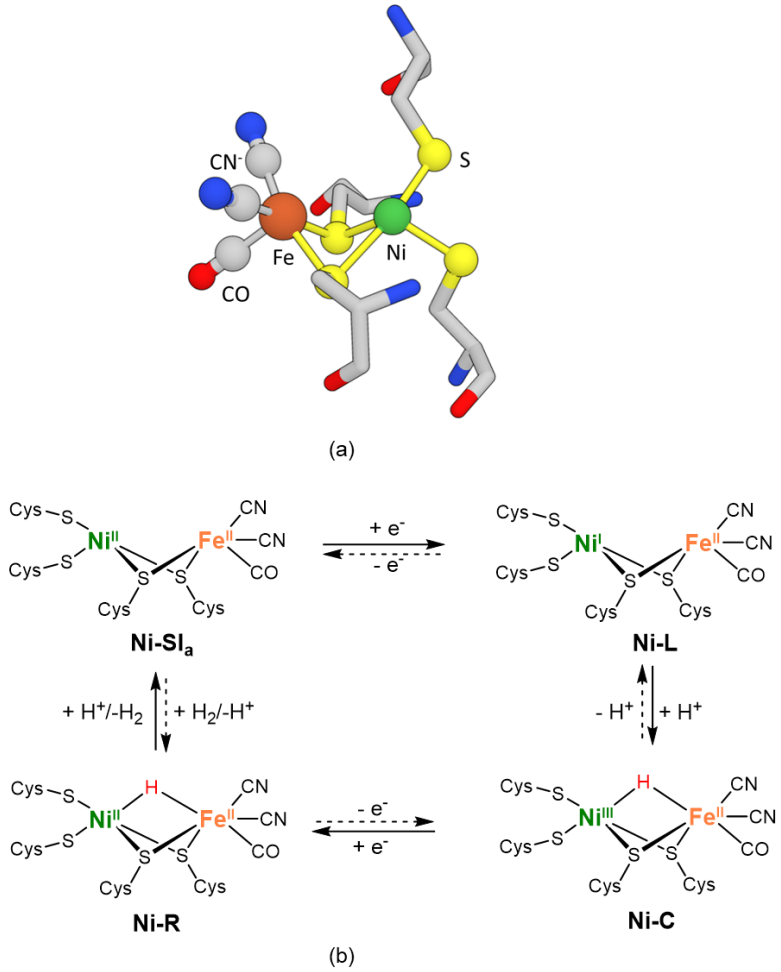

Fig. 2. (a) Structure of the [NiFe]-H_2ase active site (PDB 6EHQ) and (b) proposed catalytic cycle.

Until 2015, there has been a general agreement that only three intermediate species (of the four shown in Fig. 2b) are involved in the catalytic cycle. When H_2 production is concerned, the first intermediate is a paramagnetic Ni–C state [39, 40] ($Ni^{III}\mu(H)Fe^{II}$), generated by reaction between the resting diamagnetic Ni–SI_a state ($Ni^{II}Fe^{II}$), one electron and one proton. Ni–C is then further reduced to yield the diamagnetic Ni–R species [41, 42] ($Ni^{II}\mu(H)Fe^{II}$). Finally, protonation of Ni–R allows to release H_2 and to restore the initial Ni–SI_a. More recently, it has been established that the Ni–L state ($Ni^{I}Fe^{II}$), previously observed during low-temperature photolysis of Ni-C [43], is also involved in the catalytic cycle as intermediate between Ni–SI_a and Ni–C (Fig. 2b) [44, 45]. In both Ni–C and Ni–R, the hydride ligand bridges the two metal centers in an asymmetrical fashion with the shorter bond toward the nickel atom.

The Ni center is the key catalytic player not only because it supports the hydride, but also because the redox chemistry of [NiFe]-H_2ase is nickel-centered, with the Ni oxidation states

ranging from +I to +III during catalysis [46]. Although the Fe center remains at the +II oxidation state throughout the catalytic cycle, it synergistically contributes in the stabilization and activation of the hydride in the two intermediates Ni-C and Ni-R. In addition, the electronic impact of the strong-field ligands CO (σ-donating, π-back-bonding) and CN^- (σ-donating) at iron partly compensates the electronic changes occurring at nickel during catalysis. This is made possible by the electronic communication between the two metal ions mediated by the two thiolate bridges, but also by a direct Ni-Fe bond in Ni-L [47] and by the bridging hydride in Ni-C and Ni-R.

Inspired by the intriguing structure of H_2ase active sites, bioinorganic chemists have developed a number of synthetic [FeFe] and [NiFe] model systems showing H_2 evolution and/or oxidation activities [13-17, 48-50]. Concerning [FeFe]-H_2ase mimics, the majority of the synthetic model complexes have been designed to reproduce the {Fe2S2} core, especially the iron-iron electronic interaction and the bridging dithiolate ligand. Efforts have been also focused on the incorporation in the second coordination sphere of a proton relay, by employing an azadithiolate bridging ligand [51], and/or an electron transfer mediator, such as an $[Fe_4S_4]$ cluster [52] or a ferrocenyl group [53]. Regarding NiFe mimics, efforts were mainly dedicated on designing a {NiFeS2} core, where the Ni atom is located in a thiolate-rich environment. The Fe site has been designed with the main objective of localizing the redox activity at the Ni site with the use of CO, CN^-, Cp^-, or carbene co-ligands [54-56]. In this review, we will discuss selected structural and functional mimics of both enzymes for which the synergistic effects between the two metal centers have been highlighted.

Among the large number of [FeFe]-H_2ase mimics, Rauchfuss and co-authors reported a rather spectacular study on the symmetric complex [(dppv)(OC)Fe^I(adt)Fe^I(dppv)(CO)] ([**FeFe1**], Fig. 3a) that combines an electron-rich bimetallic core and a pendant base. The authors succeeded in crystallizing the corresponding doubly protonated compound [(dppv)(OC)Fe^{II}(adtH)Fe^{II}(*t*-H)(dppv)(CO)]$^{2+}$ ([**FeFe1**(*t*-H)H]$^{2+}$), providing unique insights into the proposed enzymatic intermediate $H_{hyd}H^+$ [57] (Fig. 1). The structure replicates the naturally relevant bridging CO and displays a strikingly short NH···HFe distance of 1.88(7) Å, indicating significant proton-hydride bonding. The [**FeFe1**(*t*-H)H]$^{2+}$ complex catalyzes HER at moderate overpotential (0.51 V) and impressive rates (TOF of 58 000 s^{-1}). During catalysis, it is proposed that [**FeFe1**(*t*-H)H]$^{2+}$ is first reduced at the Fe center with no hydride ligand (named Fe_p^{model} in Fig. 3) to generate a mixed valence H_2 intermediate. This step illustrates the role of Fe_p^{model} that, like Fe_p in the enzyme, participates to redox activity without directly interacting with the substrate.

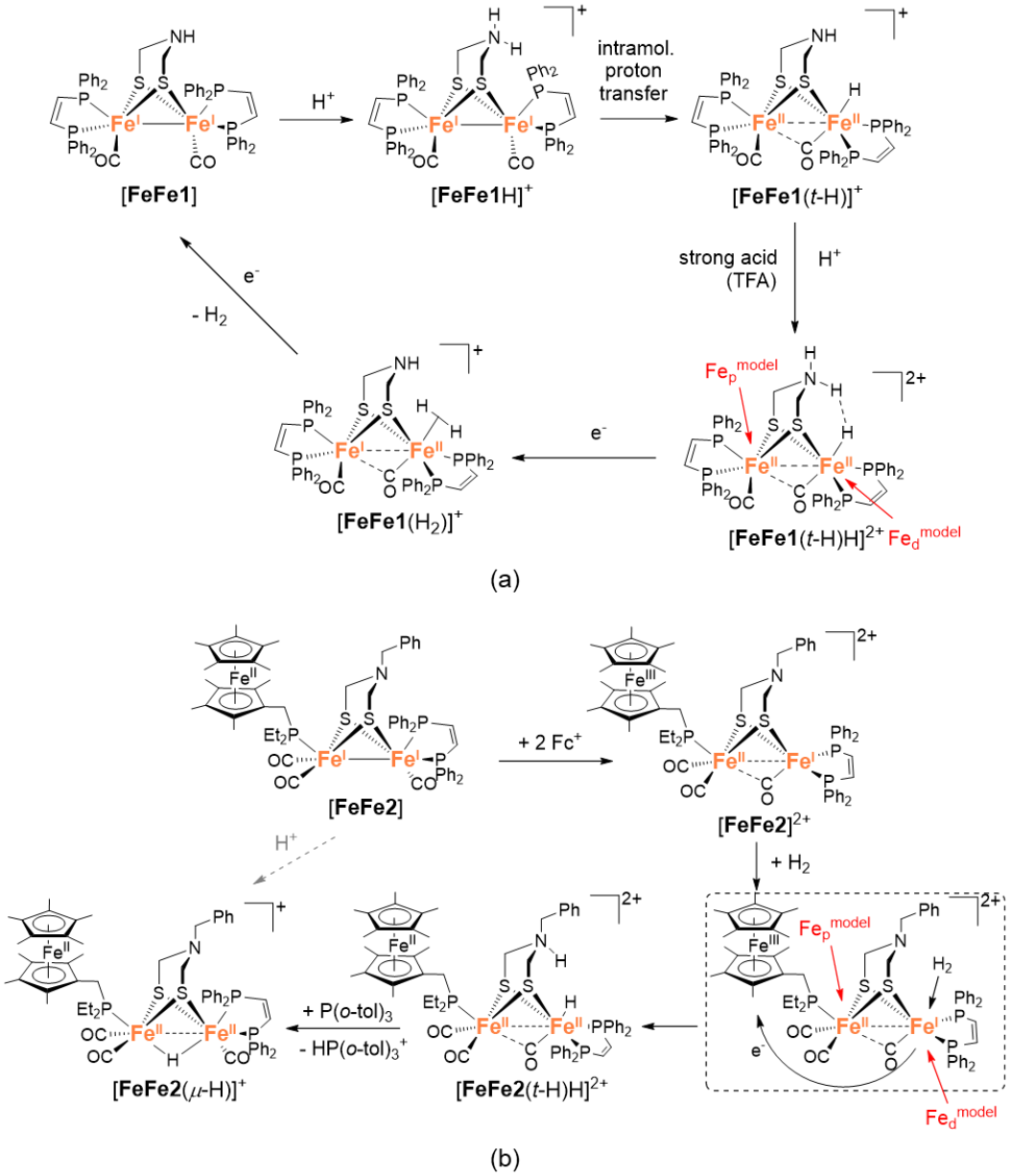

Fig. 3. (a) Proposed catalytic cycle for electrochemical H_2 production by [**FeFe1**] with strong acids, and (b) H_2 oxidation reactivity by [**FeFe2**].

The first model bearing the three essential components for catalytic activity, i.e. an active diiron center, a proton relay and a redox module, is the complex $[(Fc^{II}P^*)(CO)_2Fe^I(adt^{Bn})Fe^I(CO)(dppv)]$ ([**FeFe2**], FcP* = $Cp^*Fe(C_5Me_4CH_2PEt_2$, Bn = CH_2Ph, dppv = *cis*-$C_2H_2(PPh_2)_2$, Fig. 3b) reported by Camara and Rauchfuss [53]. The authors showed that the suitably modified ferrocene FcP* mimics the function of the $[Fe_4S_4]$ cluster. The [**FeFe2**] complex (**$Fc^{II}Fe^IFe^I$**) can be two-electron oxidized by addition of Fc^+ (2 equiv.) to generate [**FeFe2**]$^{2+}$ ($Fc^{III}Fe^{II}Fe^I$). [**FeFe2**]$^{2+}$ can then activate H_2 to produce the hydride adduct [**FeFe2**(*t*-H)H]$^{2+}$ ($Fc^{II}Fe^{II}Fe^{II}$) *via* intramolecular electron transfer from the distal iron (Fe_d^{model})

to the oxidized FcP* unit. The [**FeFe2**(*t*-H)H]$^{2+}$ species can be further deprotonated with tri(*o*-tolyl)phosphine (P(*o*-tol)$_3$) to yield the bridging hydride [**FeFe2**(μ-H)]$^+$ (that can also be produced by direct protonation of [**FeFe2**]). Most importantly, in the presence of an excess of Fc^+ used as oxidizing agent and of P(*o*-tolyl)$_3$, [**FeFe2**]$^{2+}$ catalytically oxidizes H_2 resulting in the complete conversion of Fc^+ to Fc and P(*o*-tolyl)$_3$ to [HP(*o*-tolyl)$_3$]$^+$ (TOF = 0.4 h^{-1}). A +200 mV redox potential shift of the [FcP*]$^{+/0}$ couple upon coordination to the diiron subunit reflects the electronic communication between these two moieties as in the natural H-cluster with the proximal iron mediating the electron transfer between the electron reservoir (the ferrocenyl ligand) and the distal iron.

The design and synthesis of heterobimetallic [NiFe]-H_2ase models with redox reactivity located at the Ni center has been a challenging task for bioinorganic chemists. The model [Ni^I(xbsms)(μ-CO)(μ-S)Fe^I(CO)$_2$('S')], [**NiFe1**] (H_2xbsms = 1,2-bis(4-mercapto-3,3-dimethyl-2-thiabutyl)benzene) reported by Lubitz and co-authors was the first in 2012 displaying reversible protonation of a terminally Ni-bound thiolate [58] (Fig. 4a). In addition, DFT calculations suggested the interconversion between the afforded Ni^{I}Fe^I thiol complex, [**NiFe1**SH]$^+$, with a Ni^{II}Fe^{II} μ-hydride tautomer, [**NiFe1**(μ-H**)**]$^+$, the latter having slightly higher free energy [13] (∼5 kcal mol^{-1}). Both initial ([**NiFe1**]) and protonated ([**NiFe1**SH]$^+$) compounds proved to be active for electrocatalytic H_2 evolution from trifluoroacetic acid (TFA) in acetonitrile with a 540–570 mV overpotential and a TOF of 8 h^{-1}. The poor basicity of [**NiFe1**], which is not completely protonated by TFA, is proposed to be responsible for its moderate performance. On the mechanistic side, the authors proposed that [**NiFe1**SH]$^+$ is a key intermediate to release H_2. Even if sulfur protonation takes place at the Ni site, it significantly impacts the electronic structure of the iron center, as evidenced by combined spectroscopic and DFT studies. In both [**NiFe1**] and [**NiFe1**SH]$^+$, the synergetic electronic interaction between nickel and iron is promoted by Ni-Fe σ-bonding (bond lengths: 2.426 Å and 2.433 Å, respectively) and further mediated by one CO ligand. Indeed, one CO bridges the two metals in [**NiFe1**] and becomes semi-bridging and displaced towards iron in [**NiFe1**SH]$^+$, which partly compensates the electronic changes at nickel due to sulfur protonation. The potential formation of the bridging hydride tautomer ([**NiFe1**(μ-H**)**]$^+$) also highlights the essential role of iron in the generation of hydride species.

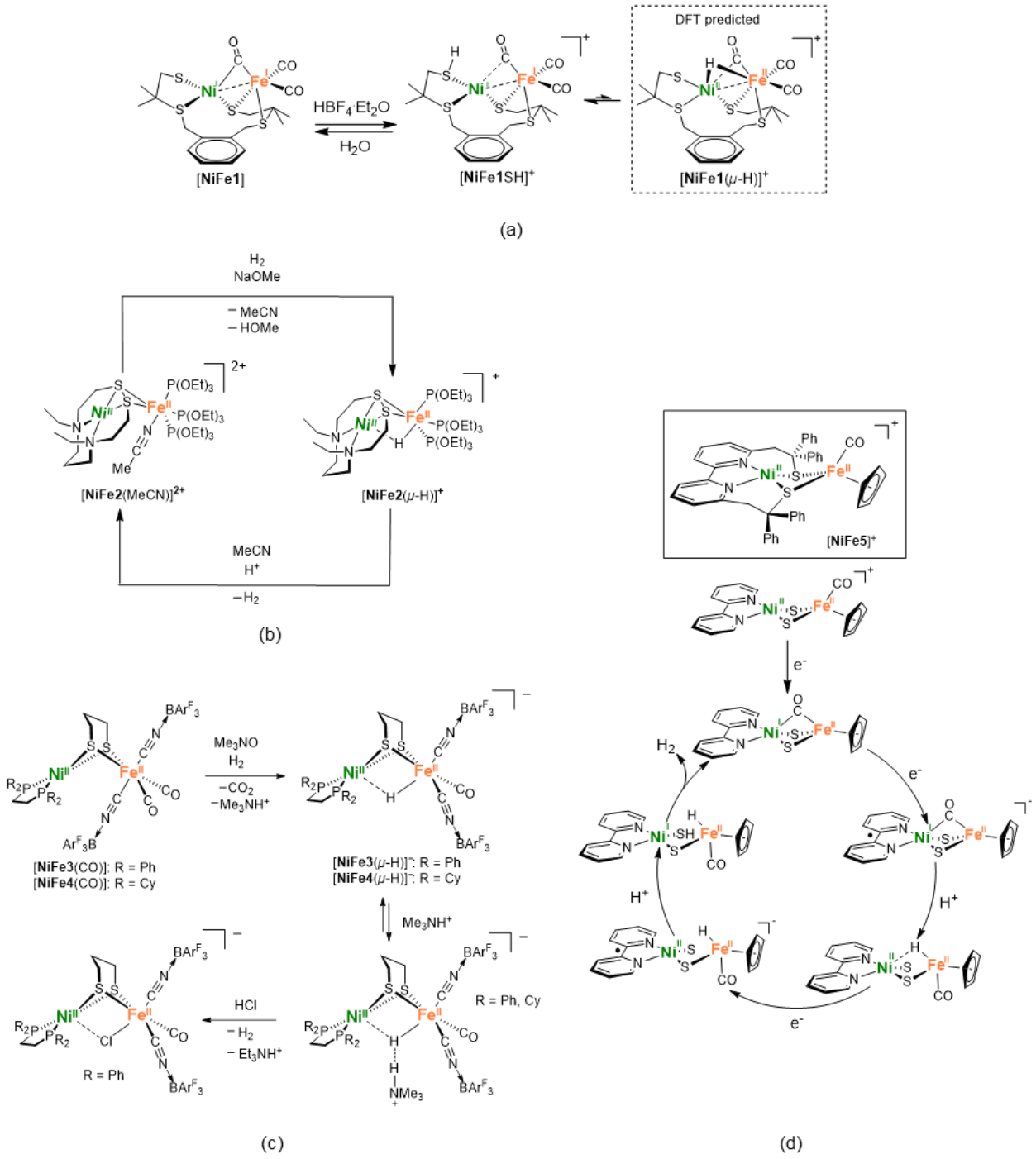

Fig. 4. Reactivity of the discussed [NiFe]-H_2ase model complexes: (a) interconversion between thiol and hydride tautomers formed from [**NiFe1**]; (b) H_2 activation by [**NiFe2**(MeCN)]$^{2+}$ affords the hydride complex [**NiFe2**(μ-H)]$^{+}$ that regenerates [**NiFe2**(MeCN)]$^{2+}$ after protonation (single turnover); (c) H_2 activation with in situ generated coordinatively unsaturated $Ni^{II}Fe^{II}$ species affords hydride models for Ni-R; (d) proposed catalytic pathway for H_2 evolution mediated by [**NiFe5**]$^{+}$ (a simplified representation of the complex is shown in the cycle).

The Ogo group reported the first nickel–iron model $[Ni^{II}(L)Fe^{II}(MeCN)\{P(OEt)_3\}_3]^{2+}$ ([**NiFe2**(MeCN)]$^{2+}$, L = N, N'-diethyl-3,7-diazanonane-1,9-dithiolato) Fig. 4b) that showed both H_2 evolution and oxidation activities, thus mimicking the bidirectional behavior of the native enzyme [59] (Fig. 4b). In acetonitrile/methanol solution, complex [**NiFe2**(MeCN)]$^{2+}$ was found to heterolytically cleave H_2 in the presence of methanolate (that captures a proton), resulting in a bridging hydride complex, [**NiFe2**(μ-H)]$^+$, with the μ-H displaced towards the iron center. Complementarily, when [**NiFe2**(μ-H)]$^+$ reacts with a strong acid (HBF_4), H_2 and the starting compound [**NiFe2**(MeCN)]$^{2+}$ are regenerated to complete a single turnover. Unlike the active site of [NiFe]-H_2ase, reactivity takes place at the Fe center and the Ni assists the process by (i) modulating the electronic properties of the $\{FeS_2\{P(OEt)_3\}_3\}$ core *via* the bis(thiolate) bridge, and (ii) stabilizing the Fe-bound hydride through the formation of an asymmetrical bridge.

In the meantime, Rauchfuss and co-authors also prepared synthetic hydride compounds by H_2 activation with even higher fidelity to the Ni-R state, in both structure and function. The two models $[(dxpe)Ni^{II}(pdt)Fe^{II}(CO)_2(CNBAr^F{}_3)_2]$ [60] (pdt = propanedithiolate; dxpe = dppe = 1,2-bis(diphenylphosphino)ethane: [**NiFe3**(CO)]; dxpe = dcpe = 1,2-bis(dicyclohexylphosphino)-ethane: [**NiFe4**(CO)], Fig. 4c) carry two borane-protected biomimetic cyanide ligands that electrophilically activate the iron center. Upon decarbonylation with Me_3NO, the [**NiFe3**(CO)] adduct, despite its lack of a positive charge, can extract H^- from H_2 to generate [**NiFe3**(μ-H)]$^-$. [**NiFe3**(μ-H)]$^-$ and its dcpe analogue [**NiFe4**(μ-H)]$^-$ are the first [NiFe]-H_2ase models containing both CN^- and H^- ligands. Except one supplementary CO in the basal plane, the Fe coordination sphere in [**NiFe3**(μ-H)]$^-$ well reproduces that in Ni-R, including a dihydrogen bonding interaction (with triethylammonium, Fig. 4c). Nevertheless, the H^- ligand remains closer to Fe (1.516 Å) than to Ni (1.710 Å), although the asymmetry is less pronounced than in [**NiFe2**(μ-H)]$^+$. The [**NiFe3**(μ-H)]$^-$ adduct, in the presence of a base (DBU) in dichloromethane solution, catalyzes electrochemical H_2 oxidation, whereas strong acids like HCl induce H_2 release. The reactivity of [**NiFe3**(μ-H)]$^-$, as of [**NiFe2**(μ-H)]$^+$, is mainly centered on the Fe site. The one-electron oxidation of the [**NiFe3/4**(μ-H)]$^-$ hydrides also occurs at the iron center to form a $Ni^{II}(\mu$-H)Fe^{III} species, in contrast to the Ni−C oxidation into Ni−R that is localized at the nickel site. These findings point to the limitations of diphosphines as mimics for the terminal ligands of the nickel ion: the presence of stronger donors is required to ensure that Ni^{II} is more easily oxidized than Fe^{II}. In these models, the Ni site seems to be required to modulate the electronic properties of the Fe coordination sphere. Actually, although decarbonylation leaves the iron center coordinatively unsaturated, the hydride ligand remains coordinated to both

nickel and iron with almost symmetrical bridging fashion ($r_{Fe–H}$ = 1.51 Å and $r_{Ni–H}$ = 1.71 Å) instead of binding terminally to the more electrophilic iron center.

With the aim of relocating redox chemistry at the Ni center, some of the authors of this review reported a heterobinuclear NiFe mimic, $[L^{N2S2}Ni^{II}Fe^{II}Cp(CO)]^+$ ($[\mathbf{NiFe5}]^+$, L^{N2S2}: Fig. 4d, Cp = cyclopentadienyl), formed by linking a neutral Ni^{II}-N2S2 complex supported by a bipyridine–bisthiolate ligand, with a {FeCpCO} precursor used as a surrogate for the $\{FeCO(CN)_2\}$ moiety of [NiFe]-H_2ase [61]. In the mononuclear Ni^{II}-N2S2 complex, coordination of nickel to the bipyridine unit allows a stabilization of the Ni^{I} and the Ni^{III} states (by delocalization of the electronic density between Ni and the bipyridine unit), thus increasing the potential for Ni-centered redox chemistry in the target heteronuclear NiFe complex. The {NiFeS2} core of $[\mathbf{NiFe5}]^+$ is almost identical to that of the resting state of the [NiFe]-H_2ase, and $[\mathbf{NiFe5}]^+$ is an active electrocatalyst for H_2 production in acetonitrile solution in the presence of a weak acid (Et_3NHBF_4, k_{cat} = 2.5(3)·10^4 $M^{-1}{\cdot}s^{-1}$ and TOF = 250 s^{-1} at η = 690 mV, 16 TONs after bulk electrolysis). The authors isolated and experimentally characterized a $Ni^{I}Fe^{II}$ and a $Ni^{II}Fe^{II}$ hydride species, mimicking two intermediates of the enzymatic cycle. A theoretical mechanistic investigation carried out by Hall and co-author revealed that (i) the first hydride intermediate to be formed shows the H^- ligand bridged between Fe and Ni, but slightly displaced towards iron, and (ii) thiolate hemilability/protonation are involved in the catalytic cycle. A consensus was reached on an E[ECEC] catalytic mechanism (E = electron transfer, C = chemical reaction), involving three reductions and two protonation steps (Fig. 4d). Such a catalytic cycle, involving decoupled electron and proton transfers, is similar to that proposed for the enzyme (ECEC), except that one more reduction step is required for the synthetic catalyst. Most importantly, the redox chemistry is Ni-centered (also with participation of the bipyridine ligand), whereas the iron center has a double role: it modulates the redox properties of nickel (two successive reductions are observed for $[\mathbf{NiFe5}]^+$, while only one is accessible for the parent mononuclear Ni complex), and supports the formation of hydride intermediates. The relevance of ligand design in this system is confirmed by the fact that when replacing the Fe-bound cyclopentadienyl (Cp) with pentamethylcyclopentadienyl (Cp*), the mechanism varies from E[ECEC] to E[CEEC], with the first $Ni^{I}Fe^{II}$ intermediate that is protonated before further reduction [62]. Besides, catalytic/mechanistic studies carried out after replacing Ni by Fe in the metallodithiolate ligand [63] suggest that the non-innocent redox L^{N2S2} ligand has a strong impact on the reactivity of the dinuclear metal core.

All of these reports clearly illustrate how, in the bimetallic active sites of the [FeFe]- and [NiFe]-H_2ases as well as in the corresponding model complexes, the two metal centers cooperate to

reversibly reduce protons to dihydrogen (or to oxidize H_2). Concerning the [FeFe]-H_2ases, biochemical and bio-inspired studies suggest that one iron acts as the binding site for substrates, when the other site assists the process synergistically in different ways: (i) modulating the electronic properties and reactivity of the active iron center, (ii) positioning the proton relay and the open coordination site in close proximity to promote H_2 release/uptake, (iii) mediating electron transfer between an "external" redox module and the active iron center. However, the mechanism of [FeFe]-H_2ases is still under debate and further efforts are required to optimize catalysis with bio-inspired complexes in terms of efficiency and stability. To reach this challenging objective, the design of a protective and functional second coordination sphere around the bimetallic core could be an interesting approach. In the case of the [NiFe]-H_2ases, the redox chemistry is nickel-centered and iron mainly contributes to the stabilization of hydride ligation and in modulating the electronic properties of nickel *via* the bis-thiolate bridge. Shifting the chemistry towards the Ni site in synthetic mimics is still puzzling. In particular, further ligand design and use of stronger donors in the coordination sphere of nickel seem to be required to displace towards nickel not only the redox chemistry but also hydride formation.

3. Dioxygen reduction: bio-inspiration from the heterobinuclear heme-copper site of C*c*O

Dioxygen (O_2) is critical for sustaining most forms of life on the Earth, in the industry and for emerging energy technologies. Despite its abundance, O_2 must be activated in order to exploit its oxidizing power, due to the chemical inertness of its fundamental triplet state. Dioxygen activation, which is generally promoted by transition metals, is a prerequisite for its proton-assisted reduction, i.e. for the Oxygen Reduction Reaction (ORR) [64]. The four-electron ORR process (Eq. 2a), generating water from O_2, is central in aerobic respiration [65] and for the production of electrical energy in fuel cells [66-68]. The two-electron ORR process (Eq. 2b) allows the production of hydrogen peroxide (H_2O_2), an environmentally benign and versatile oxidizing agent.

$$O_2 + 4H^+ + 4e^- \rightarrow 2H_2O \qquad (2a)$$

$$O_2 + 2H^+ + 2e^- \rightarrow H_2O_2 \qquad (2b)$$

Transition metal-based molecular ORR catalysts include multimetallic centers, in which synergistic effects between metal ions can promote O_2 activation and reduction. Among them, the "heme-copper Binuclear Center" (BNC) is the active site of heme−copper oxidase enzymes, which include the popular mitochondrial cytochrome *c* oxidase (C*c*O) of the respiratory chain.

These enzymes are responsible of the reduction to water of more than 90% of the dioxygen "respired" by living beings [69, 70]. In C*c*O, the free energy released by O_2 reduction (Eq. 2a, with ferrocytochrome *c* as electron source) is coupled to power trans-membrane proton pumping across the inner mitochondrial membrane, from the mitochondrial matrix to the intermembrane space [65]. The generated proton electrochemical gradient across the membrane is successively exploited to drive the synthesis of adenosine triphosphate (ATP) by the ATP synthase.

Mitochondrial C*c*Os are large multisubunit proteins containing the catalytic BNC site and two electron transport centers: a dimetallic Cu_A complex ($Cu^{1.5}Cu^{1.5}/Cu^{I}Cu^{I}$) and a low-spin six-coordinated heme *a* (Fe^{III}/Fe^{II}) [65, 71]. The BNC of C*c*O in its fully reduced state (R state, Fig. 5) contains two redox active transition metal ions: (i) a high-spin heme Fe^{II} (heme *a3*) and (ii) a Cu^{I} ion (Cu_B) located 5.1 Å apart from heme *a3* on the distal side. A histidine residue is axially-tethered to heme *a3* on the proximal side (i.e. pointing away from Cu_B) to complete the iron coordination sphere, whereas Cu_B is ligated in a T-shaped geometry by three histidine residues, one of which cross-linked to a functionally critical tyrosine.

The currently accepted catalytic mechanism of C*c*O [65, 71, 72] (Fig. 5) is divided in an oxidative phase, during which the O-O bond of dioxygen is cleaved, and a reductive phase, during which the reduced state of the enzyme (R) is regenerated.

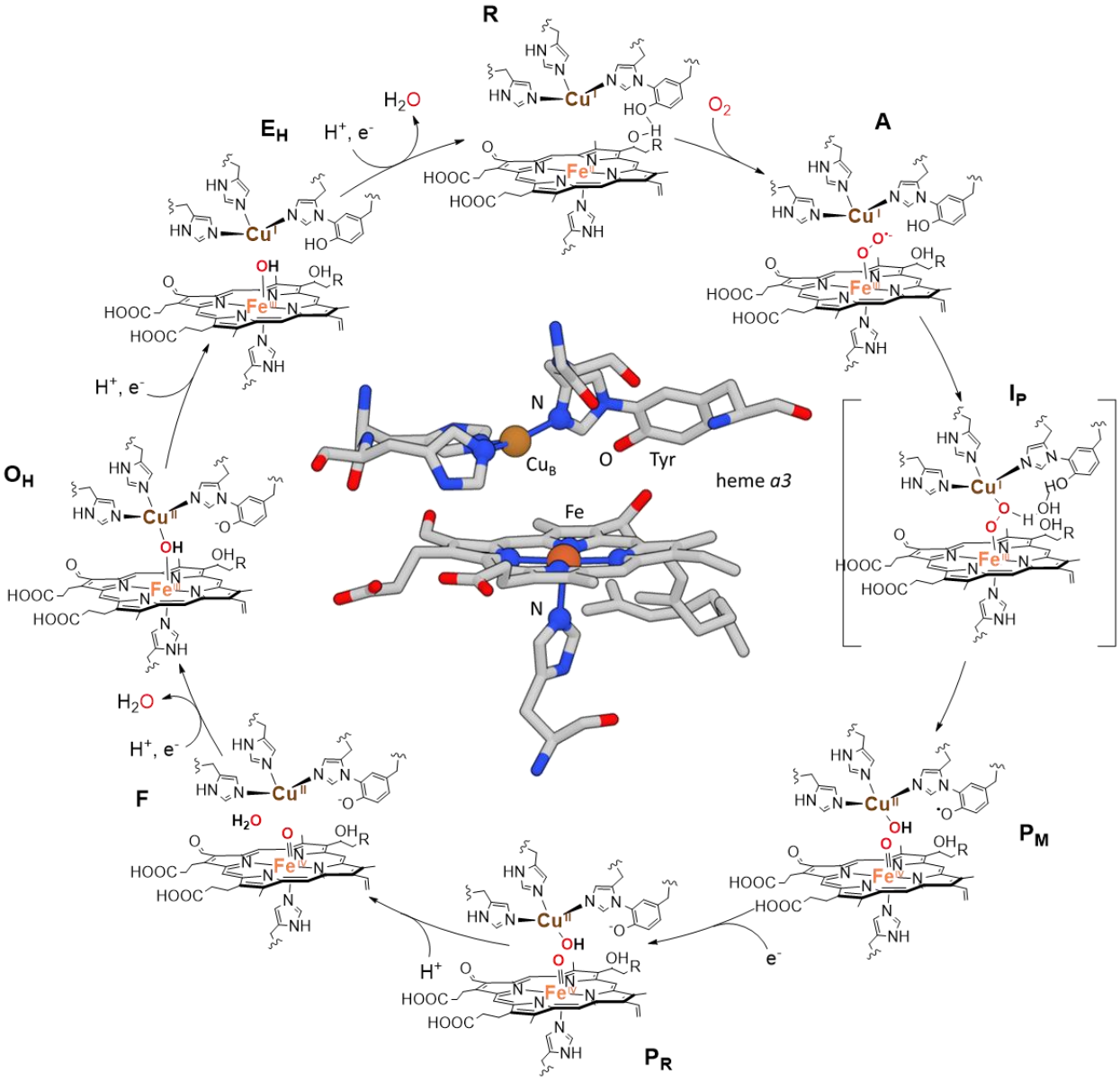

Fig. 5. Structure of the C*c*O BNC (PDB 5XDX) and currently accepted catalytic cycle for $4H^+/4e^-$ O_2 reduction.

The first step involves O_2 binding to Fe^{II} in axial position (*trans* to the Fe-bound histidine), and its activation to form a terminal "end on" Fe^{III}-η_1-superoxide species ("heme-oxy" intermediate A). Therefore, dioxygen is directly activated by Fe^{II}. However, infrared data suggest that intermediate A is generated *via* a transient Cu-O_2 state [73, 74], which induces protein conformational changes that increase the affinity of heme *a3* for O_2. This highlights how the presence of both metal sites in the C*c*O active site is essential.

The following step consists in the homolytic cleavage of the superoxide O-O bond of A to generate the P_R intermediate containing an Fe^{IV}=O heme (ferryl) and a Cu^{II}-OH unit. This step

may involve the transient formation of the P_M species. The difference between P_M and P_R is the oxidation state of the functional tyrosine, which is in its radical form in P_M and in its anionic state (tyrosinate) in P_R. It is remarkable that upon binding to iron, dioxygen accepts four electrons at once to generate $P_{M/R}$, three of them from the synergistically-operating redox active metal centers (one from Cu_B, $Cu^I \rightarrow Cu^{II}$, and two from heme *a3*, $Fe^{II} \rightarrow Fe^{IV}$), and the last one alternatively from heme *a* (in P_R) or from tyrosine (in P_M). This multi-electronic transfer is most likely the reason for the fast O-O cleavage, which precludes the detection of a (hydro)peroxo intermediate in the path from A to $P_{M/R}$. However, the transient generation of a species in which a (hydro)peroxo is bridging between iron and copper (I_P in Fig. 5) has been proposed based on DFT calculations [75, 76] and data obtained on synthetic models (see below). The bridging coordination mode of the (hydro)peroxo unit in I_P is thought to promote the homolytic rupture of the O-O bond to form $P_{M/R}$. Indeed, in the copper-free terminal Fe^{III}–OOH intermediate found in the cytochrome P450, the O-O bond cleavage occurs heterolytically [72, 77]. The direct participation of copper to the O-O bond breaking event can be thus proposed.

The reductive phase of the mechanism, i.e. the regeneration of the R state from P_R, involves the addition of four protons and three electrons to the active site. This process is coupled to the uptake and pumping of protons from the inner to the outer side of the mitochondrial membrane in a not completely understood way. Three intermediates have been observed during this phase: (i) the F state, which corresponds to another oxyferryl (Fe^{IV}=O) species generated by protonation of the Cu_B-bound hydroxo ligand of P_R, with concomitant release of water; (ii) the O_H state, formed from F by addition of one proton and one electron, for which the exact attribution is uncertain (it may be a Fe^{III}–OH$\cdots$$Cu^{II}$ tyrosinate as in Fig. 5, or a Fe^{III}–OH$\cdots$$Cu^{I}$ tyrosine radical state, or these two species could coexist in equilibrium); and (iii) the E_H state, a Fe^{III}–OH Cu^I tyrosinate intermediate generated by one electron reduction of O_H. The catalytic cycle is then completed by an additional proton-coupled electron-transfer on E_H, leading to the regeneration of the R state and the release of a second water molecule.

The C*c*O active site is attractive for model chemistry, including biosynthetic and synthetic models. These two approaches have contributed to support the essential role of heme-copper synergy for biological dioxygen reduction to water. Among biosynthetic C*c*O mimics, we focus on a series of myoglobin mutant proteins, here named M_BMb, containing (i) a high-spin heme cofactor with an axial His ligand and a high O_2-binding affinity as in C*c*O, as well as (ii) a tris-histidine/glutamate binding pocket (non-heme M_B site) on the distal side of the heme. The M_B site is related to the Cu_B site of C*c*O and can be metallated with Cu^I (like in C*c*O), Fe^{II} or the redox-inactive Zn^{II}. Studies on M_BMb models provide insights on (i) why a non-heme metal

ion is required in C*c*O and, (ii) why copper is preferred over iron in this site [78]. The O_2 reduction rates (*k*) and selectivity for water production (*S*) for the Cu^{I}, Fe^{II}, and Zn^{II}-M_BMb derivatives have been determined: $k_{Cu^{I}}$ = 2.72(10) $\mu M \cdot s^{-1}$, $S_{Cu^{I}}$ = 94%; $k_{Fe^{II}}$ = 1.15(7) $\mu M \cdot s^{-1}$, $S_{Fe^{II}}$ = 96%; $k_{Zn^{II}}$ = 0.22(2) $\mu M \cdot s^{-1}$, $S_{Zn^{II}}$ = 57%. From these data the Cu-variant of M_BMb is the most active one, in accordance with the "choice" of nature for copper in C*c*O. Besides, spectroscopic, electrochemical and theoretical studies on Cu^{I}, Fe^{II}, and Zn^{II}-M Mb allowed to gain further insights on the role of the non-heme metal in C*c*O.

(i) The higher ν(Fe–O_2) frequency observed in the resonance Raman spectrum of the "heme-oxy" adduct from Zn^{II}-M_BMb *vs* naked M_BMb (594(28) vs 575(25) cm^{-1}, respectively) suggests that the presence of a non-heme metal ion increases the Fe–O_2 bond strength, making the O–O bond weaker and thus enhancing O_2 activation.

(ii) The presence of a redox-active metal ion (Cu^{I}, Fe^{II}) in the tris-histidine/glutamate binding pocket has a stronger beneficial effect on ORR activity (*k*, see above) than a non-redox one (Zn^{II}). This is due to the direct electron donation of the redox metal to O_2, with Cu^{I} or Fe^{II} being oxidized to Cu^{II} or Fe^{III}, respectively (as shown by multiple spectroscopic techniques). In addition, a weaker O-O bond is predicted when the non-heme site is occupied by copper instead of iron (O-O distance of 1.391 vs 1.351 Å, respectively, in the "heme-oxy" intermediate).

(iii) The O_2 reduction rates (*k*) for the Cu^{I}-M_BMb and Fe^{II}-M_BMb models are sensitive to the concentration of electron donor, attesting how electron transfer is rate-determining. Most importantly, it was shown that the rate enhancement with increasing electron donor concentration is higher for Cu^{I}-M_BMb than for Fe^{II}-M_BMb. This suggests that copper in the non-heme site of C*c*O enables a faster electron transfer from redox centers to the BNC than iron. This could be explained by the fact that in C*c*O copper ensures a higher driving force for such electron transfer, as found with the Cu^{I}- and Fe^{II}-M_BMb models (E^0 of the Cu^{II}/Cu^{I} pair is higher than E^0 of the non-heme Fe^{III}/Fe^{II} pair, +387(25) mV vs +259(20) mV vs SHE, respectively). However, it cannot be excluded that the reorganization-energy difference between copper and iron may also play a role.

Synthetic models of the C*c*O catalytic center are limited to heterobinuclear heme-copper complexes that reproduce to some extent the structural motif and reactivity of the BNC. From a functional point of view, these models can be classified into two categories: (i) mimics reproducing stoichiometric dioxygen (or dioxygen-relevant) reactivity of the BNC and enabling the access to metal-dioxygen intermediates potentially relevant for BNC chemistry (such as metal-peroxo, -superoxo and -oxo/hydroxo species); and (ii) catalytic models, i.e. heme-copper complexes that promote catalytic $4H^{+}/4e^{-}$ ORR [72, 79].

Synthetic model chemistry of the BNC was exhaustively reviewed [72, 80]: here, we focus on selected examples that are pertinent for highlighting the importance of iron-copper synergy. Stoichiometric models are based on either (i) molecular assemblies with separated heme and copper units connected through an activated oxygen derivate (mostly peroxo), or (ii) the use of a ligand that covalently links the Fe-heme and copper units. A first heme–peroxo–copper complex belonging to the second class, $[(DCHIm)(tacn^{Acr})Fe^{III}(O_2)Cu^{II}]^+$ (**FeCu1** in Fig. 6, $tacn^{Acr}$ = 1,4,7-triazacyclononane-capped picket fence porphyrinate, DCHIm = 1,5-dicyclohexylimidazole), was reported by Collman and co-authors [81].

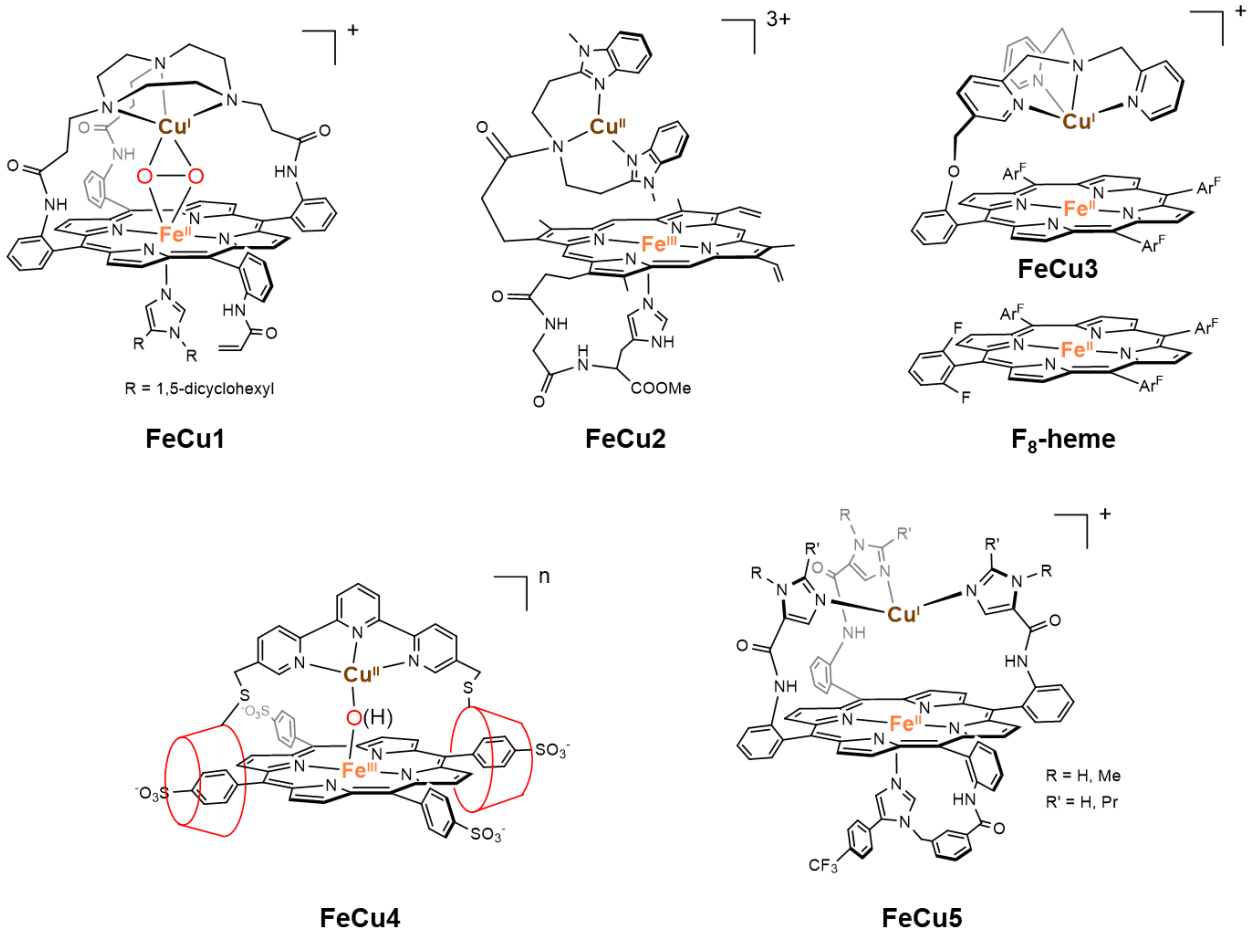

Fig. 6. Heme-copper C*c*O BNC mimics discussed in the text (the corresponding Fe-only species are analogues but Cu-free; the mononuclear **Fe$_8$-heme** complex is also shown for comparison with **FeCu3**; in **FeCu4** the red truncated cones represent per-O-methylated β-cyclodextrins).

It was obtained by irreversible reaction of dioxygen with the corresponding Fe^{II}-Cu^{I} precursor, in the presence of an excess of DCHIm, and assigned to a μ-η^2:η^2 ("side on") bridging peroxo complex. The essential role of copper in the reactivity is supported by the fact that the corresponding iron-only complex (i.e. with no metal in the tacn pocket) reacts with dioxygen

much more slowly and in a reversible way. In another example of heme/Cu systems reported by Casella and co-authors, $[(HMGH)Fe^{III}Cu^{II}]^{3+}$ (HMGH indicates the employed multitopic ligand; **FeCu2** in Fig. 6), the heme was functionalized with a chelating moiety for copper and an imidazole for axial coordination to iron [82]. From reactivity studies, the authors suggested a manifold of roles for copper: (i) a "cooperative" role, the Fe^{III}/Cu^{II} complex displaying greater affinity for azide coordination than its iron(III)-only analogue; (ii) a protective role, since the thermal degradation of the Fe/Cu–O_2 adduct formed by reaction of the reduced complex (Fe^{II}-CO/Cu^{I}) with O_2 is slower than for the Fe-only O_2-adduct; and (iii) a reactivity booster role, since **FeCu2** catalyzes *p*-cresol peroxidation with enhanced kinetics compared to the Cu-free catalyst. The peroxidase activity was also evaluated with Fe^{III}, Co^{II}, Mn^{II}, or Zn^{II} in the non-heme site [83]. In all cases, the non-heme metal ion was shown to enhance catalytic activity, with the greatest effects observed for the redox active metals.

All catalytic C*c*O models are ORR electrocatalysts working in aqueous solutions [72]. There is only one exception reported by Fukuzumi, Karlin and co-authors. They described a heme/Cu-tpa assembly ($[(heme^{tpa})Fe^{II}Cu^{I}]^{+}$, **FeCu3** in Fig. 6, tpa = tris(2-pyridylmethyl)amine) and its Fe-only analogue, both acting as homogeneous 4-electron ORR catalysts in air-saturated acetone solution, at low and room temperature (−60 °C < T < −5 °C and 25 °C, respectively), in the presence of TFA as proton source and of $Me_{10}Fc$ as electron donor [84]. Kinetic measurements evidenced that O_2 binding is the rate-determining step at 25 °C (while the O-O cleavage is limiting at −60 °C). Therefore, the fact that at room temperature the ORR rate with the Fe-Cu catalyst is twice the rate with the Fe-only catalyst agrees with an active role of copper in promoting O_2 binding to heme, and not necessarily in inducing O−O bond cleavage. This result is consistent with C*c*O investigation supporting a role of Cu_B as the initial coordination site for dioxygen in the BNC [73, 74]. In parallel, electrocatalytic O_2 reduction was explored with **FeCu3** and derivates immobilized on edge plane pyrolytic graphite (EPG) [85]. A comparison of the Faradaic efficiency for O_2 reduction to water for the Fe/Cu complex (74%), the Fe-only analogue (59%) and the parent F_8-heme platform (lacking the tpa-containing function, 20%) evidences a beneficial effect of copper for 4-electron reduction. The low selectivity for H_2O observed with the F_8-heme is proposed to result from the formation of a heme-peroxo-heme intermediate that is known to easily release H_2O_2 in acidic water.

Kitagishi and co-authors reported a supported ORR electrocatalyst based on a supramolecular complex formed between an iron(III)-porphyrinate derivative and two per-*o*-methylated *β*-cyclodextrin molecules connected *via* a (2,2´:6´,2´´-terpyridyl)copper(II) complex linker (Fe^{III}TPPS/Cu^{II}TerpyCD_2 or **FeCu4,** Fig. 6, TPPS = 5,10,15,20-tetrakis(4-

sulfonatophenyl)porphinato, CD = per-O-methylated β-cyclodextrin) [86]. The electrocatalytic performances of this Fe/Cu assembly, confined in the hydrophobic pocket of the β-cyclodextrins, were compared with those of the copper-free system. In the presence of copper, catalytic current densities increase more than twice and the selectivity is notably modified in favor of $4H^+/4e^-$ ORR (3.0 electron reduction for the Fe/Cu assembly vs 1.6 electron reduction for the Cu-free system, as determined by rotating disk voltammetry). This last observation suggests that Cu^I in the terpyridyl Cu complex acts as an electron source, as proposed for Cu_B in C*c*O [87-89].

Among the different ORR electrocatalysts studied in the Collman's lab [64], a family of EPG-deposited biomimetic heme/Cu complexes incorporates three imidazolyl ligands for copper binding and an imidazolyl axial ligand to complete the heme iron coordination, as found in the *CcO* catalytic site [90-92]. All these catalysts are selective for $4H^+/4e^-$ ORR. Among them, those shown in Fig. 6 and named **FeCu5** showed outstanding catalytic performances (more than 10000 turnovers at physiologically relevant pH and potential >50 mV vs NHE). Under these non-biologically relevant conditions of fast electron flux (from the EPG electrode to the catalyst), the presence of copper did not significantly affect the ORR turnover frequency, and only improves slightly the selectivity (from >90% for the Fe-only compound to >96-98% for the Fe/Cu assemblies). Interestingly, the **FeCu5** compounds (vs Fe-only analogues) were also investigated under diffusion-limited electron flux conditions by incorporation of diluted catalyst solutions into a lipid matrix deposited on the electrode surface [93]. Under these biologically relevant conditions, the Fe/Cu catalysts (still selective for $4H^+/4e^-$ ORR) maintain their catalytic activity and stability, while it is not the case for the Fe-only species. This can be rationalized by considering the biomimetic role of copper(I) as an electron reservoir. Actually, Cu^I can act as reductant for high valent oxygen species (such as ferryl or $Fe^{IV}=O^{+\cdot}$) and can thus prevent their accumulation that could damage the supporting ligand under slow electron transfer conditions.

All these investigations demonstrate how in the heterobimetallic center of C*c*O, as well as in the corresponding synthetic and biosynthetic models, two redox active metal centers (one heme iron and one copper ion) cooperate to activate and reduce dioxygen to water. In C*c*O the heme moiety is directly responsible for O-O bond reductive activation and rupture, while the copper site assists the process in at least three synergetic ways: (i) promoting O_2 binding to iron through the transient formation of a Cu-O_2 adduct; (ii) facilitating electron transport to the catalytic center; (iii) directly participating to the O-O bond cleavage step (i.e. the conversion of the I_P intermediate to $P_{M/R}$).

Other multimetallic transition metal complexes that are not directly inspired from the BNC site of C*c*O are able to activate and reduce dioxygen [64, 80]. In particular, a few dimetallic complexes, including homodimetallic dicopper [94-96], dicobalt [97, 98], dimanganese [99], diiron [100], and heterodimetallic ruthenium/nickel species [101, 102] have been reported as homogeneous $2H^+/2e^-$ or $4H^+/4e^-$ ORR (electro)catalysts. Among them, the case of cofacial cobalt macrocycles is emblematic to illustrate how synergy between two metal centers (even of the same type), can have strong impact on O_2 chemistry. Fukuzumi, Guilard and co-authors reported a single-bridged cofacial cobalt(II) porphyrin catalyst, [Co_2(DPX)] (**Co_2^{DPX}**, DPX = diporphyrin xanthene, Fig. 7) that is selective for $4H^+/4e^-$ ORR, in contrast to the parent mononuclear Co^{II}-porphyrin (**Co^{OEP}**) that is selective for $2H^+/2e^-$ ORR under the same conditions ($HClO_4$, ferrocenes, benzonitrile solution) [103]. To rationalize this mismatch, the authors suggested that in this specific cofacial system the formation of a bridged Co^{III}-O-O-Co^{III} intermediate promotes O-O bond cleavage and thus the production of water, while the same pathway is not available for the mononuclear analogue. However, the bridging spacer properties (length and orientation of the macrocycle substituents) in cofacial dimetallic complexes are critical to address ORR selectivity. In another example reported by Cook and co-authors [104], an arene-ruthenium(II) clipped tetrabridged cofacial Co^{II} porphyrin, [Ru^{II}_8(η_6-iPrC_6H_4Me)$_8$(dhbq)$_4$(Co^{II}TPyP)$_2$][OTf]$_8$ (**Co-prism**, Co^{II}TPyP = Co^{II} tetra(meso-4-pyridyl)-porphyrinate, dhbq = 2,5-dihydroxy-1,4-benzoquinato, Fig. 7) was reported to reduce O_2 to H_2O_2 with a 90% selectivity (trifluoroacetic acid, ferrocene, benzonitrile solution). Note that **Co-prism** also displays a ~ten-fold faster kinetics compared to the related mononuclear compound (**Co^{TPyP}**), as a consequence of the "face to face" arrangement. Very recently, Cao and co-authors have reported a very efficient and selective $4H^+/4e^-$ ORR catalyst based on an asymmetric cofacial cobalt porphyrin-porphyrin dyad, the dinuclear Co^{II} triphenylporphyrin-tri(pentafluorophenyl)porphyrin complex [105] (**$Co_2^{TPP,TPFP}$**, Fig. 7). In a H_2SO_4 aqueous solution, **$Co_2^{TPP,TPFP}$** loaded on carbon nanotubes showed higher ORR performances in terms of overpotential and selectivity (η = 0.51 V, 3.9 electron reduction) compared to the corresponding mononuclear Co porphyrins (**Co^{TPP}** and **Co^{TPFP}**, Fig. 7) and to all reported symmetrical dinuclear Co bis(porphyrins) (including the parent dinuclear Co^{II} bis(tri(pentafluorophenyl)porphyrin)) complex, **$Co_2^{(TPFP)2}$**, Fig.7). The asymmetrical structure is thought to be responsible for the improved activity of **$Co_2^{TPP,TPFP}$**: while the redox-active Co-TPFP porphyrin unit is in charge of the binding and activation of O_2, the Co-TPP site remains at the Co^{III} state and serves as Lewis acid to assist catalysis. More specifically, Co^{III}-TPP stabilizes the first (TPFP)Co^{III}-$O_2^{\cdot-}$ intermediate electrostatically and supports the

successive peroxo-bridged intermediate. In a similar way to bis(porphyrins), synergy between two metal ions has been also exploited in various ORR electrocatalysts based on bis(corroles) and porphyrin−corrole dyads [106].

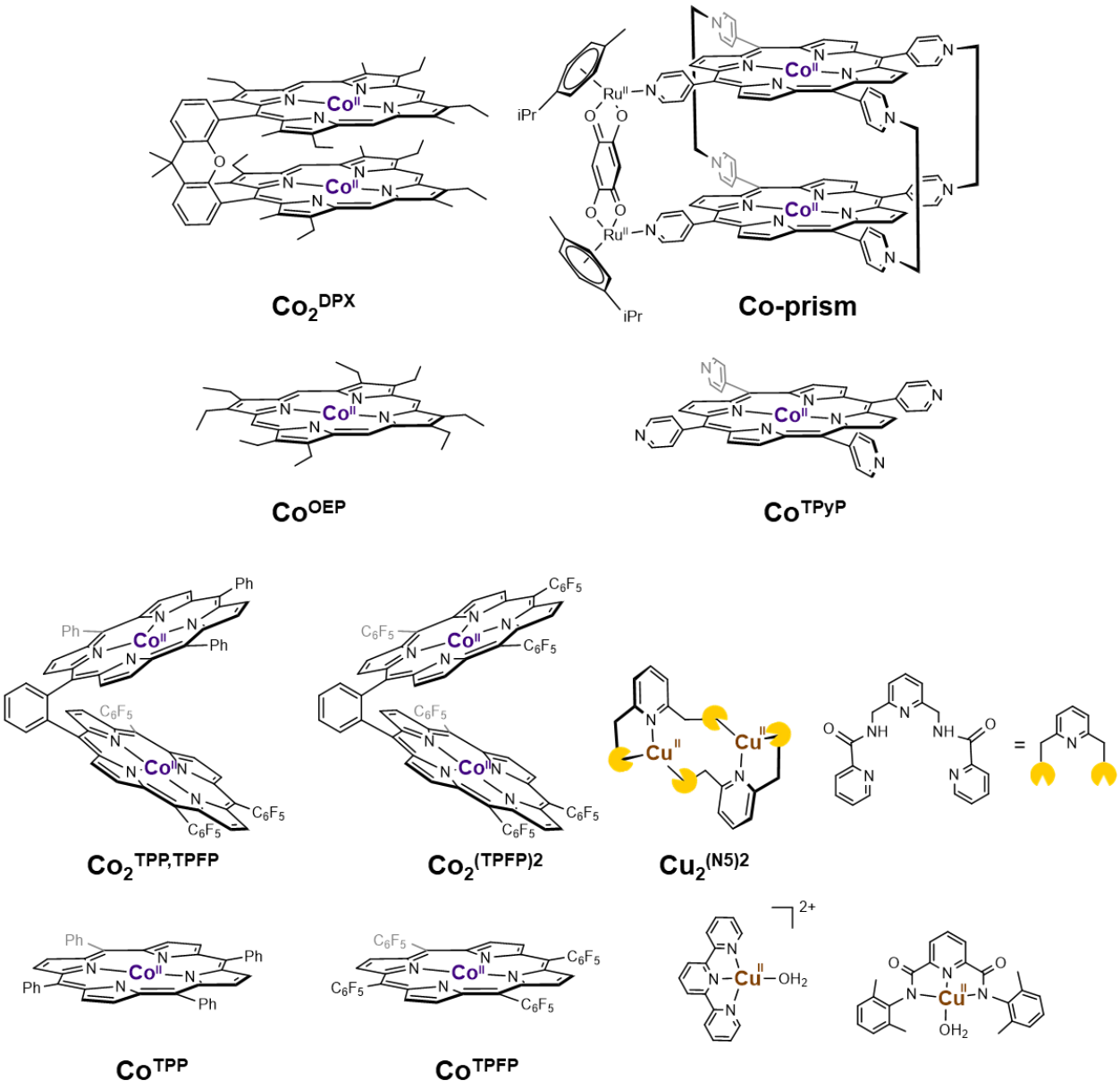

Fig. 7. Examples of multimetallic ORR catalysts not directly inspired from the BNC site of C*c*O, with the corresponding mononuclear analogues (second and fourth rows). In **Co-prism**, only one of the four spacers is shown.

Among the different examples of multinuclear non-macrocyclic systems, a dimetallic copper complex supported by a pentadentate polypyridine–polyamide ligand (**$Cu_2^{(N5)2}$**, Fig. 7), reported by Cao and co-authors, well highlights the essential contribution of dinuclearity for orienting the selectivity towards $4H^+/4e^-$ ORR in late transition metal complexes [96]. More

specifically, at -0.9 V *vs* NHE in neutral water, **$Cu_2^{(N5)2}$** behaves as an homogeneous ORR electrocatalyst with 3.95 transferred electrons per O_2 molecule, whilst only 2.77-2.91 electrons are transferred when parent mononuclear Cu complexes (Fig. 7) are used under the same conditions. The cooperation between the two Cu ions in **$Cu_2^{(N5)2}$** is therefore crucial to promote the bimetallic homolytic O–O bond cleavage for $4H^+/4e^-$ ORR. Such a mechanism is not accessible in mononuclear late transition metal complexes, which usually catalyze $2H^+/2e^-$ ORR.

All these examples of O_2-reducing polynuclear complexes, bio-inspired by the C*c*O or not, demonstrate that multimetallic catalysis and metal-metal synergy can have a strong impact on ORR selectivity and/or kinetics by affecting geometries and energies of transition states and by enabling alternate bimetallic reduction pathways that are not accessible for their mononuclear counterpart(s). However, there is still a need of systematic studies to determine the electronic or/and structural factors that control the selectivity and tune the catalytic efficiency of the ORR process.

4. The carbon cycle: the essential role of CO dehydrogenase and acetyl-coenzyme A synthase for CO_2/CO fixation

In nature, carbon monoxide (CO) and carbon dioxide (CO_2) enter the metabolism of many aerobic and anaerobic organisms and are fixed into organic carbon. In the anaerobic Wood Ljungdahl (WL) pathway, one of the most efficient paths for CO_2 fixation, two CO_2 molecules are converted into one acetyl-SCoA molecule ($^-$SCoA = co-enzyme A) in the presence of protons, electrons and $^-$SCoA. The last two steps of the process (Eq. 3 and 4), catalyzed by NiFe-dependent CO dehydrogenase (NiFe-CODH) and acetyl-coenzyme A synthase (ACS) [107, 108], are essential reactions of tremendous interest in industry, i.e. the reverse water gas shift reaction and the Monsanto process, respectively. NiFe-CODH catalyzes CO_2 reduction into CO (Eq. 3), while ACS the successive formation of a C-C bond between the generated CO and a methyl group bound to the Co center of a B_{12}-containing protein, followed by a thioesterification with $^-$SCoA to generate acetyl-SCoA (Eq. 4).

$$CO_2 + 2H^+ + 2e^- \leftrightarrows CO + H_2O \quad (3)$$

$$CO + [Co^{III}]\text{-}CH_3 + {}^-SCoA \leftrightarrows CH_3\text{-}CO\text{-}SCoA + [Co^{I}] \quad (4)$$

In some aerobic or anaerobic organisms that use CO as the sole source of carbon, CO is first

oxidized into CO_2 (Eq. 3), which is then fixed into carbohydrates through the Calvin-Benson-Basham pathway. Two CODHs can be involved to oxidize CO into CO_2: the above-mentioned NiFe-CODH (in this case, not associated to ACS) in the anaerobic organisms and the MoCu-CODH in the aerobic organisms [109].

It is remarkable that the active sites of the NiFe-CODH, MoCu-CODH and ACS all contain multinuclear centers exploiting metal-metal cooperation for substrate activation. The NiFe-CODH enzyme contains five (or seven) metal clusters per homodimeric enzyme, including three (or five) electron transport [Fe_4S_4] clusters and two NiFe sulfur clusters, named C-clusters, where the reaction (CO_2 reduction/ CO oxidation) occurs [110-112]. The C-cluster is a [$NiFe_4S_4$] cluster, in which a Ni atom is located in one vertex of a highly distorted iron-sulfur cubane and a pendant Fe atom is attached to it. Many different forms of C-cluster have been crystallized: the initial structure (inactive form) includes a bridging sulfide between the Ni and pendant Fe centers [111, 113, 114] (Fig. 8a). In the active form of the C-cluster (C_{red1}, Fig. 8b), the Ni^{II} ion is coordinated by three sulfur ligands in a planar T-shaped geometry, while the pendant Fe^{II} ion is in a tetrahedral environment including a hydroxo ligand. During catalysis (Fig. 8), redox activity only occurs at the Ni site that cycles between Ni^{II} and Ni^{0}. In the CO oxidation direction, the $Ni^{II}Fe^{II}$ state first activates CO to generate a Ni^{II}-CO adduct (C_{red1}-CO) [115]. An Fe-bound hydroxide then reacts with Ni^{II}-CO through a nucleophilic attack to generate a bridging carboxylate between the Ni and Fe centers (C_{red1}-CO_2). The successive release of CO_2 leads to a $Ni^{0}Fe^{II}$ state (C_{red2}) that is then re-oxidized to complete the catalytic cycle. A strong synergistic effect between the Ni and the pendant Fe sites is mandatory to explain the efficiency of this enzyme: the Ni center activates the CO molecule, while the Lewis acidity of the Fe^{II} center allows the formation of the Fe-OH unit from water at physiological pH. Finally, the C cluster allows for a perfect positioning of the Fe^{II}-OH and Ni^{II}-CO units for an optimized reaction.

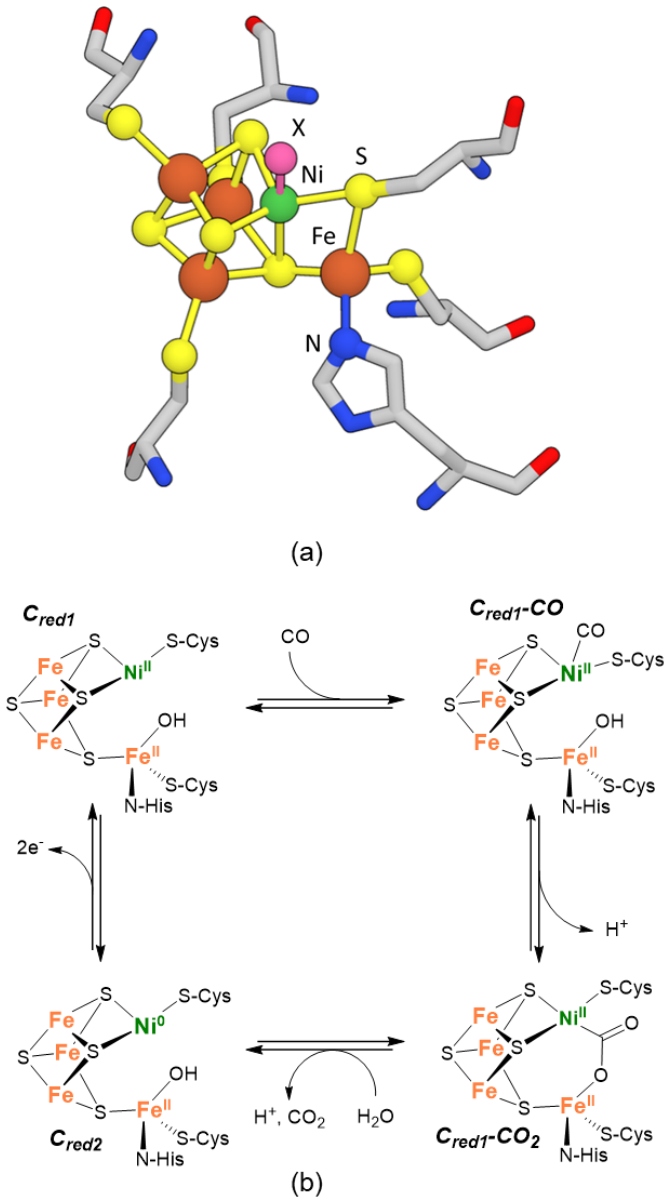

Fig. 8. (a) Structure of the NiFe-CODH active site (PDB 1JQK, inactive state, X = unknown atom) and (b) currently accepted catalytic cycle.

The MoCu-CODH enzyme is composed of three subunits, each containing two [Fe_2S_2] clusters and an active site consisting of a heterodimetallic {MoSCu} core [109, 116, 117] (Fig. 9a). In the resting state, the Mo center is coordinated in a square pyramidal geometry with an oxo ligand in the axial position, and in the equatorial plane two sulfurs from a pyranopterin cofactor, a hydroxyl group, and an unsupported sulfide bridging Mo to a Cu center. The Cu donor set is completed by only one thiolate from a cysteine resulting in an almost linear coordination geometry. The first common step in the two possible catalytic pathways currently discussed in the literature, is the two-electron oxidation of the Mo^{IV}-hydroxo unit into a Mo^{VI}-oxo species

(Fig. 9b). Based on a recent study, this oxidized form can be viewed as a frustrated Lewis pair, with the Mo^{VI}=O unit serving as the Lewis base and the Cu^{I} ion being the Lewis acid [118]. In both catalytic paths (A and B), the Mo^{VI}=O/Cu^{I} intermediate activates CO through its coordination at the copper site (Cu^{I}). As in Ni-CODH, the key step is the nucleophilic attack of the Mo^{VI}-bound oxo ligand to Cu^{I}-CO to generate a carboxylate bridging the two metal centers. To close the cycle, CO_2 is released with the concomitant coordination of another hydroxyl ion to Mo. The difference between the two proposed paths arises from the structure of the metal carboxylate intermediate: it can be bound to copper either *via* the carbon atom, or via the oxygen atom with a C···S interaction strengthening the linkage.

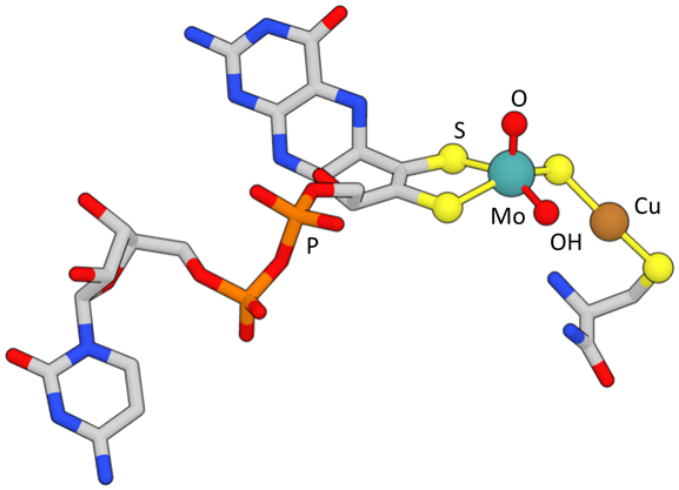

(a)

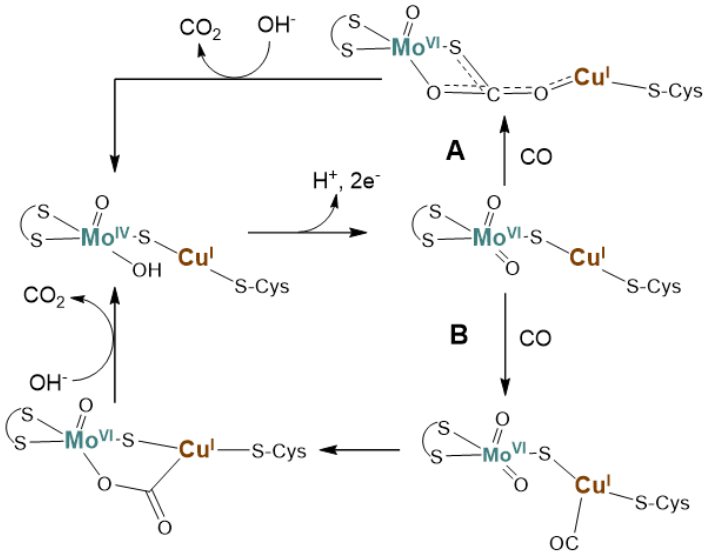

(b)

Fig. 9. (a) Structure of the MoCu-CODH active site (PDB 1N5W) and (b) currently accepted catalytic cycle.

As Ni and Fe in NiFe-CODH, Mo and Cu act in synergy, but in a slightly different way. The copper center activates CO but has formally no redox activity (it remains in the +1 oxidation state, contrarily to Ni in NiFe-CODH that switches between the +2 and 0 oxidation states). On the other hand, the Mo site combines redox activity and Lewis acid properties to generate a nucleophilic oxo ligand (while pendant Fe in NiFe-CODH is redox inactive). Besides, (i) the bimetallic arrangement supports the bridging carboxylate coordination in the Mo-μ-CO_2-Cu intermediate, and (ii) the CO_2 release step is assisted by the sulfide-mediated high electronic delocalization between copper and molybdenum.

The ACS enzyme is composed of three main subunits, one containing the active site, the second interacting with the NiFe-CODH and the last one binding $^{-}$SCoA. The active site (A-cluster, Fig. 10a) is composed of a nickel center, the so-called *proximal* nickel (Ni_p), which is linked to a $[Fe_4S_4]^{2+}$ cluster *via* a μ-thiolate and to a second Ni center, named *distal* nickel (Ni_d), *via* two μ-thiolates (all the bridging thiolates arising from cysteine residues) [108]. Substrates binding and redox activity seem to be confined to the Ni_p center, displaying coordination vacancies resulting from its T-shaped tris-thiolate coordination. In the currently proposed mechanism for ACS [115] (Fig. 10b), Ni_p switches between three different oxidation states, Ni^{I} , Ni^{II} and Ni^{III}. The first active species is generated by one electron reduction of the Ni^{II} resting state, and then activates CO to form a Ni^{I}-CO intermediate. Ni^{I}-CO is then methylated by a CH_3-Co^{III} to form a OC-Ni^{III}-CH_3 intermediate and Co^{I}. The subsequent C-C formation is triggered by an internal one-electron transfer that reduces Ni^{III} to Ni^{II}. The final step corresponds to the reductive elimination of the thioester acetyl-SCoA by reaction between the generated Ni^{II}-$C(O)CH_3$ and $^{-}$SCoA. The presence of both the $[Fe_4S_4]^{2+}$ cluster and Ni_d are proposed to assist the internal electron transfer occurring during the catalytic cycle and to stabilize the unusual T-shape structure of Ni_p, respectively. The iron-sulfur cluster and Ni_d also modulate the redox and electronic properties of Ni_p for an optimal catalytic efficiency.

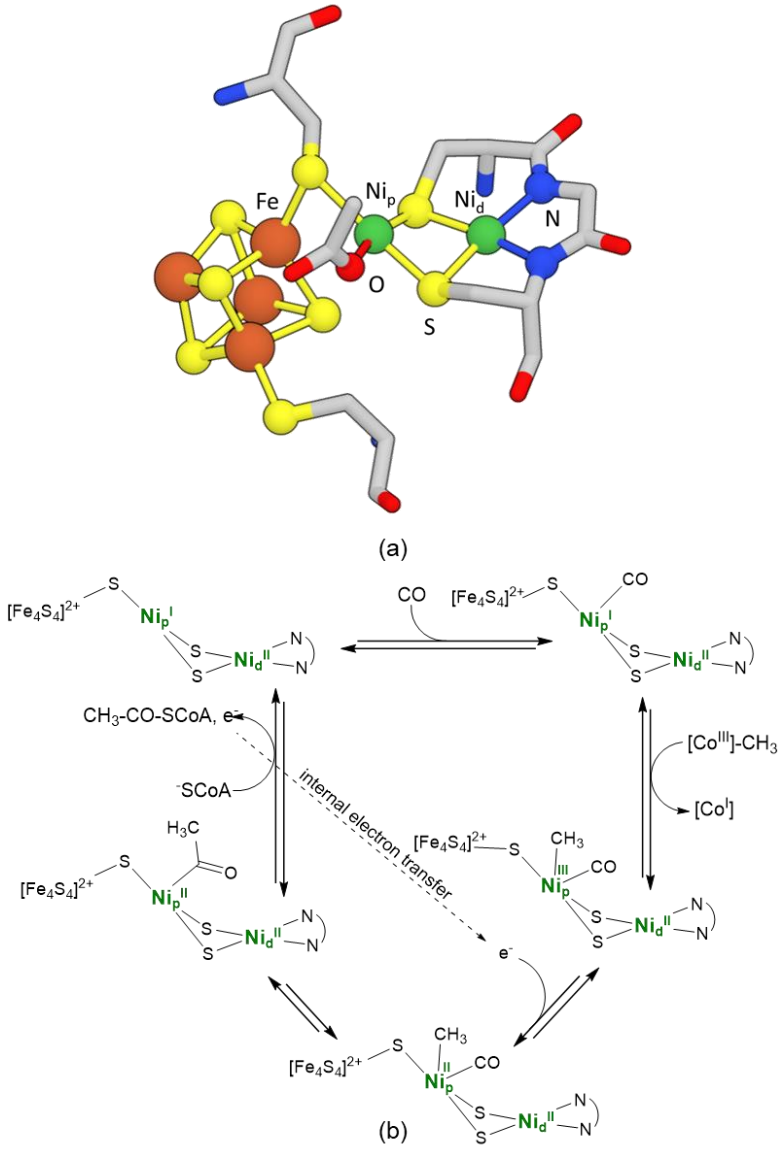

Fig. 10. (a) Structure of the ACS active site (PDB 1OAO) and (b) currently accepted catalytic cycle.

In the current societal context, CODHs and ACS should appear as great sources of inspiration for the design of CO_2 reduction and carbonylation catalysts, respectively. However, even if structural models have been described, the number of active mimics is currently very limited. In the case of the NiFe-CODH, although a large number of heterodinuclear NiFe complexes have been reported as structural and/or functional models of [NiFe]-hydrogenase (see Section 2), none have shown the ability to reduce CO_2. Note that in the quest of a better understanding of the enzyme mechanism, a complex displaying a Ni^{II}-μ-CO_2-Fe^{II} motif obtained by direct CO_2 coordination has been reported, demonstrating that such structure can be stabilized in synthetic models [119]. Regarding CO oxidation, no active heterodinuclear NiFe complexes

have been reported so far, whilst some mononuclear Ni complexes have been shown to activate CO (at the +I or 0 oxidation state). Recently, a $Ni^{II}Ir^{III}$ complex, $[Ni^{II}(X)Ir^{III}(CO)(Cp^*)]^{2+}$ (**NiIr**, X = N,N'-dimethyl-3,7-diazanonane-1,9-dithiolato), has been described capable to efficiently catalyze CO oxidation under basic aqueous conditions in the presence of 2,6-dichlorobenzeneindophenol (DCIP) as electron acceptor [120] (Fig. 11a). Several intermediate species have been characterized including a Ni^{II}-μ-CO_2-Ir^{III} complex that is generated from Ni^{II}/Ir^{III}-CO species in the presence of hydroxide. Even if CO is activated at the Ir site instead of at the Ni site as in NiFe-CODH, the formation of a carboxylate bridge between the two metal ions well illustrates their synergetic role as observed in the enzyme.

Concerning MoCu-CODH mimics, several structural {MoSCu} models have been reported, but none displays CODH reactivity [118, 121-124]. Groysman and co-authors described a MoCu complex, $[Mo^{VI}O_3Cu^{I}(L)]^{2-}$ (**MoCu**, L= (E)-3-(((2,7-di-tert-butyl-9,9-dimethyl-5-((pyridin-2-ylmethylene)amino)-9H-xanthen-4-yl)amino)methyl)benzene-1,2-diolate), in which a high valent Mo-oxo unit attacks a Cu^{I}-bound imine function through intramolecular nucleophilic addition as for the MoCu-CODH (Fig. 11b). In this case, the imine group of the supporting ligand plays the same role of CO in the enzyme, and the corresponding hydrolysis products (aldehyde and amine) are released instead of CO_2 [125]. In the absence of Cu^{I}, only traces of the products of ligand hydrolysis are formed, demonstrating that copper plays a role in positioning the imine substrate in proximity of the nucleophilic Mo–oxo and in enhancing its electrophilic character.

In the case of ACS, since only Ni_p seems to be directly involved in its reactivity, models are mainly mononuclear Ni complexes that coordinate CO and/or CH_3^+ [126-129]. Currently, there is only one dinuclear Ni complex that has been proven efficient for ACS activity. Tatsumi and co-authors have investigated the $[L^{N2S2}Ni^{II}\mu\text{-}(S_2)Ni^{0}(cod)]$ complex (**NiNi**, cod = 1,5-cyclooctadiene) that generates the methyl/thiolate adduct $[L^{N2S2}Ni^{II}\mu\text{-}(S_2)Ni^{II}(CH_3)(SDmp)]$ (Dmp = 2,6-dimesitylphenyl) by reaction with the CH_3^+ donor $[Co^{III}(dmgBF_2)_2(Me)(Py)]$ (dmg = dimethylglyoximate) and KSDmp [130, 131] (Fig. 11c). In a successive step, the addition of CO in the presence of cod excess leads to the release of the acetylthioester MeCOSDmp *via* reductive elimination regenerating **NiNi**. Using a less reactive thiolate, a relevant acyl intermediate $[L^{N2S2}Ni^{II}\mu\text{-}(S_2)Ni^{II}(COMe)(SC_6Cl_5)$ complex has been isolated, confirming that CO insertion in the Ni-methyl bond occurs before the thioesterification as proposed in the ACS mechanism. The N2S2-coordinated Ni^{II} center is not reactive, but plays a structural role to hold the two bridging sulfurs in an adequate and flexible position for optimal activity of the active

Ni center.

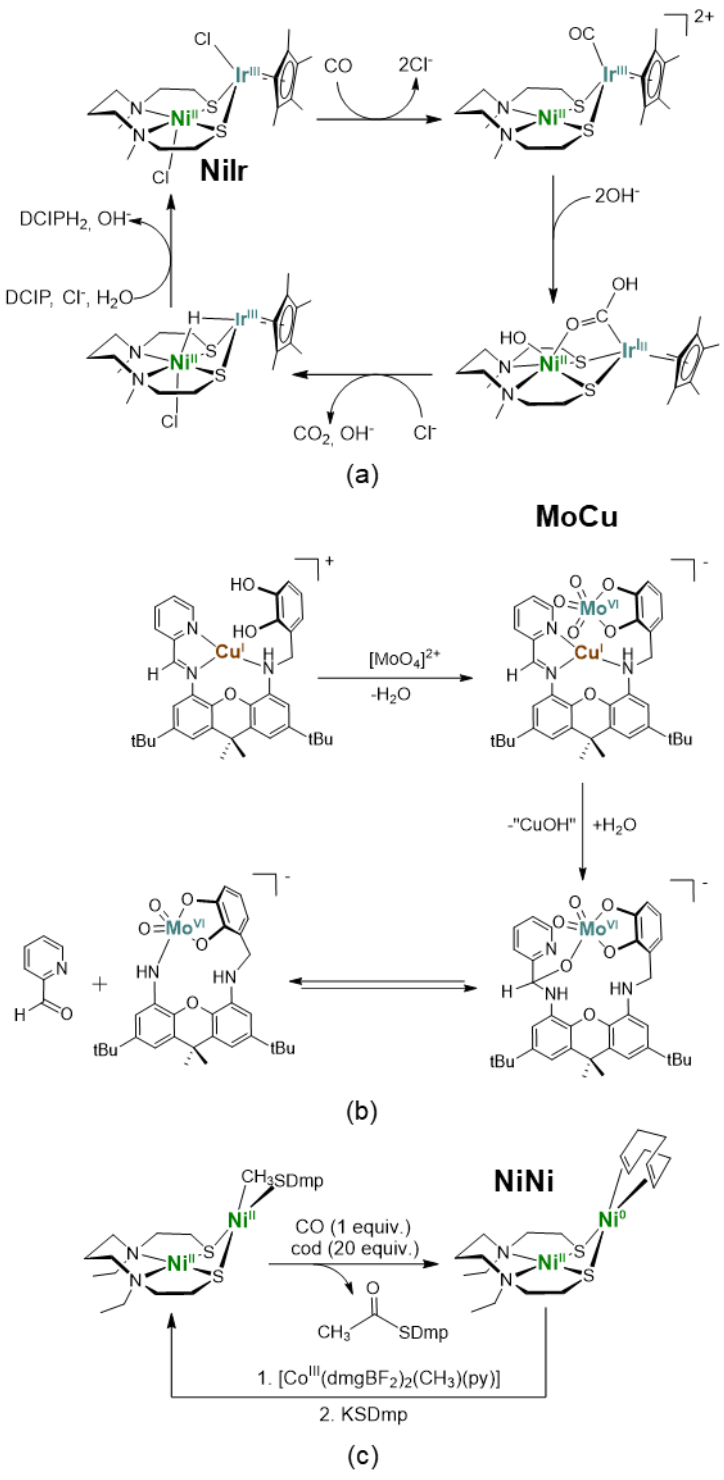

Fig. 11. Model complexes for the (a) NiFe-CODH, (b) MoCu-CODH and (c) ACS discussed in the text. In (a), the system is catalytic (all the displayed intermediates have been characterized), while in (b) and (c), this is a single turnover activity.

In summary, the active sites of the CODH and ACS enzymes are composed of clusters

containing a heterodinuclear unit essential for their activity and where each one of the metal centers fulfills a precise function. In CODHs, when considering the CO oxidation direction, one metal ion is responsible for CO binding (Ni^{II} or Cu^{I}), while the second (Fe^{II} or Mo^{IV}) generates the nucleophilic metal-bound oxo/hydroxo ligand attacking the pre-activated CO. In ACS, even if the reactivity (binding of CO and methyl group for an efficient C-C formation) is localized only on one Ni, the second Ni is required to stabilize the T-shape geometry of the active Ni and to modulate its electronic properties. To date, chemists have not succeeded to develop synthetic catalysts by mimicking these features. However, in the light of these great sources of inspiration, researches in the CO/CO_2 valorization domain should also consider the exploration of bio-inspired heterometallic clusters to reproduce the metal-metal cooperation found in these enzymes, crucial for optimal activity.

5. Dinitrogen reduction: FeMo-co of nitrogenase vs synthetic FeFe and MoMo complexes

Dinitrogen (N_2), which makes up to ~78% of the Earth's atmosphere, is essential for sustaining all living organisms. However, due to its chemical inertness it is not directly accessible to plants and animals, and hence nitrogen fixation, i.e. ammonia (NH_3) formation from nitrogen gas, is one of the most important reactions in chemistry (Eq. 5).

$$N_2 + 6H^+ + 6e^- \rightarrow 2NH_3 \qquad (5)$$

Ammonia is the main source of nitrogen fertilizers that provide food for about half of the present world population [132]. In addition, the development of "nitrogen economy" based on the use of NH_3 as an energy or hydrogen carrier, is emerging [133]. Ammonia synthesis from nitrogen gas is currently performed through the Haber-Bosch process on the surface of a K^+ promoted Fe (or Ru) catalyst [134]. Even if this process is indispensable to our society, it is highly energy consuming and strongly impacts the environment in terms of carbon footprint. Consequently, the development of more energetically and environmentally viable strategies for ammonia production from dinitrogen is required. The implementation of artificial nitrogen fixation processes based on the use of molecular catalysts under mild conditions requires to retrieve as much information as possible from biological nitrogen fixation, which is promoted by a multimetallic active site.

In nature, nitrogenases are the only enzymes known to convert nitrogen into ammonia. They work under ambient pressure and temperature using electron carriers (ferredoxins or flavodoxins) as reducing reagents and water as a proton source [135-138]. Among the different types of nitrogenases (molybdenum-, vanadium-, and iron-only), the Mo-dependent one is the most diffused, efficient and selective. From dinitrogen, protons and electrons, Mo-nitrogenase produces ammonia with the concomitant generation of dihydrogen as co-product, and the process is energetically sustained by the hydrolysis of ATP.

Crystallographic studies have confirmed that Mo nitrogenase is a multimeric protein complex composed of an electron transfer Fe protein and a N_2-fixing MoFe protein [139]. The tetrameric MoFe protein contains two catalytic units, each including an [Fe_7S_9MoC-homocitrate] cofactor called FeMo-co, where the reduction of dinitrogen to ammonia occurs, and an [Fe_8S_7] cluster (P cluster), involved in the electron transfer from the Fe protein to FeMo-co. In its resting state, the FeMo-co structure can be viewed as two cubanes, [Fe_4S_3C] and [$MoFe_3S_3C$] sharing a single carbon atom (whose identity was confirmed spectroscopically) and connected through three μ^3-bridging sulfides [137, 140] (Fig. 12a).

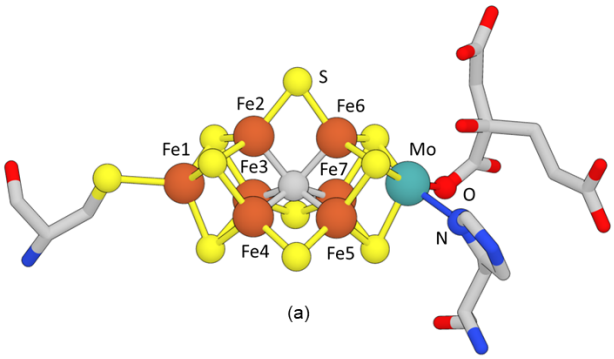

(a)

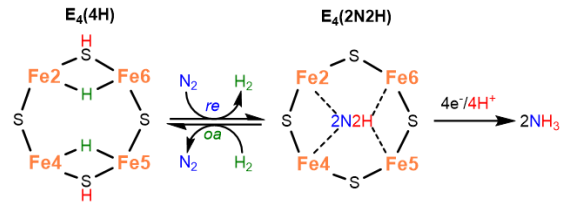

Janus intermediate (b)

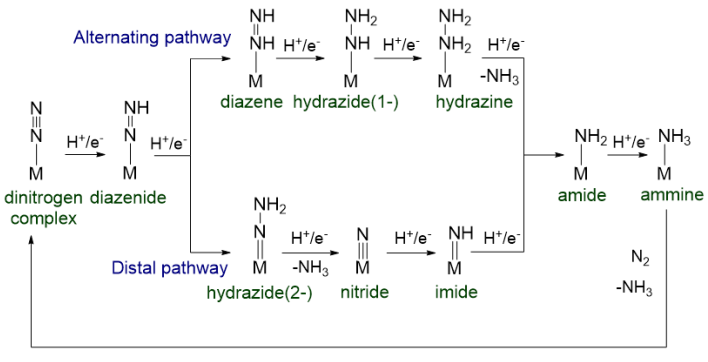

(c)

Fig. 12. (a) Structure of nitrogenase FeMo-co (PDB 4WZB), (b) currently accepted key step for biological N_2 activation, and (b) alternative pathways for N_2 reduction to NH_3 (general scheme).

The molybdenum atom is coordinatively saturated, surrounded by three bridging sulfides, one histidine, and a bidentate homocitrate, leaving no vacant site available for dinitrogen substrate binding. On the opposite vertex of the cluster, the tetrahedral S4 coordination of iron (Fe1) is completed by one terminal cysteine residue from the protein backbone. Each one of the remaining six central iron atoms (Fe2-Fe7) is coordinated by two μ^3- and one μ^2-sulfides in a trigonal pyramidal geometry, with the single C atom at the apex. Altogether, Fe2-Fe7 constitute a trigonal prism with three open Fe_4S_4 faces, capped by Fe1 and Mo and containing the C atom in its center. One of such exposed Fe_4S_4 faces is predicted to host the dinitrogen binding and reduction site since the iron atoms of this face (Fe2/4/5/6 in Fig. 12a) possess vacant coordination sites [138]. Coherently, mechanistic studies have shown that these coordinatively unsaturated iron centers are responsible for the formation of hydrides and for N_2 binding, although the precise catalytic pathway is still under debate [135, 141, 142].

During N_2 reduction catalysis, the electrons are transferred one-by-one from the Fe protein to the MoFe protein, and ultimately accumulated on FeMo-co. A "draft mechanism" proposed by Hoffman and co-authors, supported by ENDOR studies and theoretical calculations and unifying with the previous Lowe–Thorneley kinetic model [143, 144], shows how electrons and protons accumulate on FeMo-co to activate the cofactor [135, 138, 145-147]. Following this reaction path, four electrons and four protons must be accumulated on the FeMo-co resting state to generate the $E_4(4H)$ state, called the "Janus" intermediate, responsible for N_2 binding and activation (Fig. 12b). The "Janus" intermediate contains two [Fe−(μ-H)−Fe] units and two protons located on bridging sulfides [148-150]. Four coordinatively unsaturated iron sites thus cooperate for accumulating electrons on the metal cluster in the form of bridging hydrides, whilst avoiding changes in the formal oxidation state of the metal core.

Dihydrogen release from $\{E_4(4H)\}$ in a reductive elimination pathway, which is formally equivalent to the release of two protons and two electrons, makes available the two remaining reducing equivalents for N_2 coordination and the first stage of its reduction. Upon translocation of the two protons from hydrosulfides to Fe-bound N_2 a spectroscopically observed diazenido-metal complex $\{E_4(2N2H)\}$ is formed [151-153] (Fig. 12b). Its further reduction by four electrons/protons leads to formation of two equiv. of ammonia and the resting state. Two mechanistic pathways, distal and alternating [154], are commonly invoked (Fig. 12c) for this

route, which are distinguished by the sequence of proton/electron transfers on the N_2 unit and by the timing of ammonia release [135]. An "alternating" pathway is highly likely for FeMo-co because the same intermediates are spectroscopically observed when N_2, diazene or hydrazine are used as substrates [135, 147, 155-157]. Finally, despite extensive mechanistic studies, it is still not established if and how the molybdenum center [158] and the central carbide [159] influence the reactivity of the FeMo-co for N_2 binding and reduction.

Inspired by the FeMo-co reactivity and the Haber–Bosch process, in which K^+ additives are used to enhance the reactivity of the Fe-based catalyst, several transition metal complexes have been found to display nitrogen reduction activity [160-163]. Nevertheless, the number is limited only to a few examples when multimetallic systems are concerned [164-173].

Holland and co-authors reported iron complexes that support dinitrogen binding and stoichiometric N-N bond cleavage triggered by cooperation between multiple metal centers. The β-diketiminate dinuclear $[(\beta\text{-diketim})Fe^{II}Cl]_2$ complex (**$Fe_2^{diketim}$**, Fig. 13a) was shown to react with KC_8 under dinitrogen atmosphere to form a dinitride-bridged tetranuclear complex. In this compound, three of the four iron centers are required for N_2 splitting and involved in nitride coordination [166]. Combining moderate steric bulk (with methyl rather than isopropyl substituents) on the supporting ligand and interaction of the Fe-bound nitrides with a K^+ cation was the key for enabling N_2 cleavage [169, 174]. More recently, Murray and co-authors described a triiron(II) complex supported by a β-diketiminate cyclophane ligand, $[(chp^{\beta\text{-diketim}})Fe^{II}{}_3Br_3]$, (**$Fe_3^{diketim}$**, Fig. 13b) that cleaves N_2 after reduction with KC_8 [175]. The resulting trinuclear mixed valence $Fe^{II/III}$ complex contains three protonated N-atom bridges, the origin of protons being still unclear. The following addition of acids to the **$Fe_2^{diketim}$** and **$Fe_3^{diketim}$** derived N-atom bridged adducts leads to the release of (sub)stoichiometric amounts of ammonia (up to 96% [172] and 30% [175], respectively). These works highlight that both elongation and complete rupture of the N≡N bond can be promoted by cooperation between three iron atoms, each one channelling electrons to the N_2 molecule, but also by harnessing the synergy with alkali metal cations. Alkali metal cations are thought to facilitate N_2 cleavage (i) by stabilizing, *via* electrostatic interactions, highly reduced negatively charged complexes, especially the generated N-products, but also (ii) by promoting cation─π interactions with supporting ligands that contribute to locate the transition metals close enough to each other to facilitate their cooperation for N_2 activation.

The Peters group investigated dimetallic iron complexes derived from a binucleating ligand scaffold designed with a mixed phosphine−silyl−thiolate coordination environment. Among them, the [Fe{$SiP^{iPr}{}_2$(μ-SAr)}Fe] complex (**Fe_2^S**, $SiP^{iPr}{}_2$(μ-SAr) = {[(2-

$^{i}Pr_2PC_6H_4)_2Si]_2(C_6H_3S)\}^{3-}$, Fig. 13c), including an aryl thiolate function, was shown to support dinitrogen coordination to iron to afford bis-N_2 adducts $[Fe(N_2)\{Si^{iPr}{}_2(\mu\text{-}SAr)\}(N_2)Fe]^n$ (n = 0, ±1).[176] It was the first example of a sulfur-supported multinuclear complex capable of N_2 binding, since none of the previously described bio-inspired iron−sulfur clusters reminiscing the most stringent features of FeMo-co [177-180] showed interaction with N_2 [181, 182]. Interestingly, in the Peters system bis-N_2 ligation is maintained across three oxidation states (Fe^IFe^I, $Fe^{II}Fe^I$, and $Fe^{II}Fe^{II}$) [176]. The anionic $[Fe^I(N_2)\{Si^{iPr}{}_2(\mu\text{-}SAr)\}(N_2)Fe^I]^-$ system undergoes stoichiometric reduction of the bound N_2 to produce 1.8(0.3) equiv of ammonia, when treated with an excess of KC_8 and $[H(OEt_2)_2]BAr^F{}_4$. The cationic $[Fe^{II}(N_2)\{Si^{iPr}{}_2(\mu\text{-}SAr)\}(N_2)Fe^{II}]^+$ species serves as an effective pre-catalyst for hydrazine disproportionation to NH_3 and N_2 and is more active compared to the parent monometallic analogue $[Fe\{SiP^{iPr}{}_2S^{Ad}\}N_2)]^+$ (**Fe^{S}N$_2$**, Fig. 13c, 29 vs < 0.25 equiv. NH_3 h^{-1}, respectively) [183]. The N−N bond cleavage of hydrazine is probably facilitated in the bimetallic complex owing to a certain degree of cooperation between the two Fe ions in $Fe^{II}Fe^{II}$ species and/or the presence of the bridging thiolate, which could act as a proton shuttle.

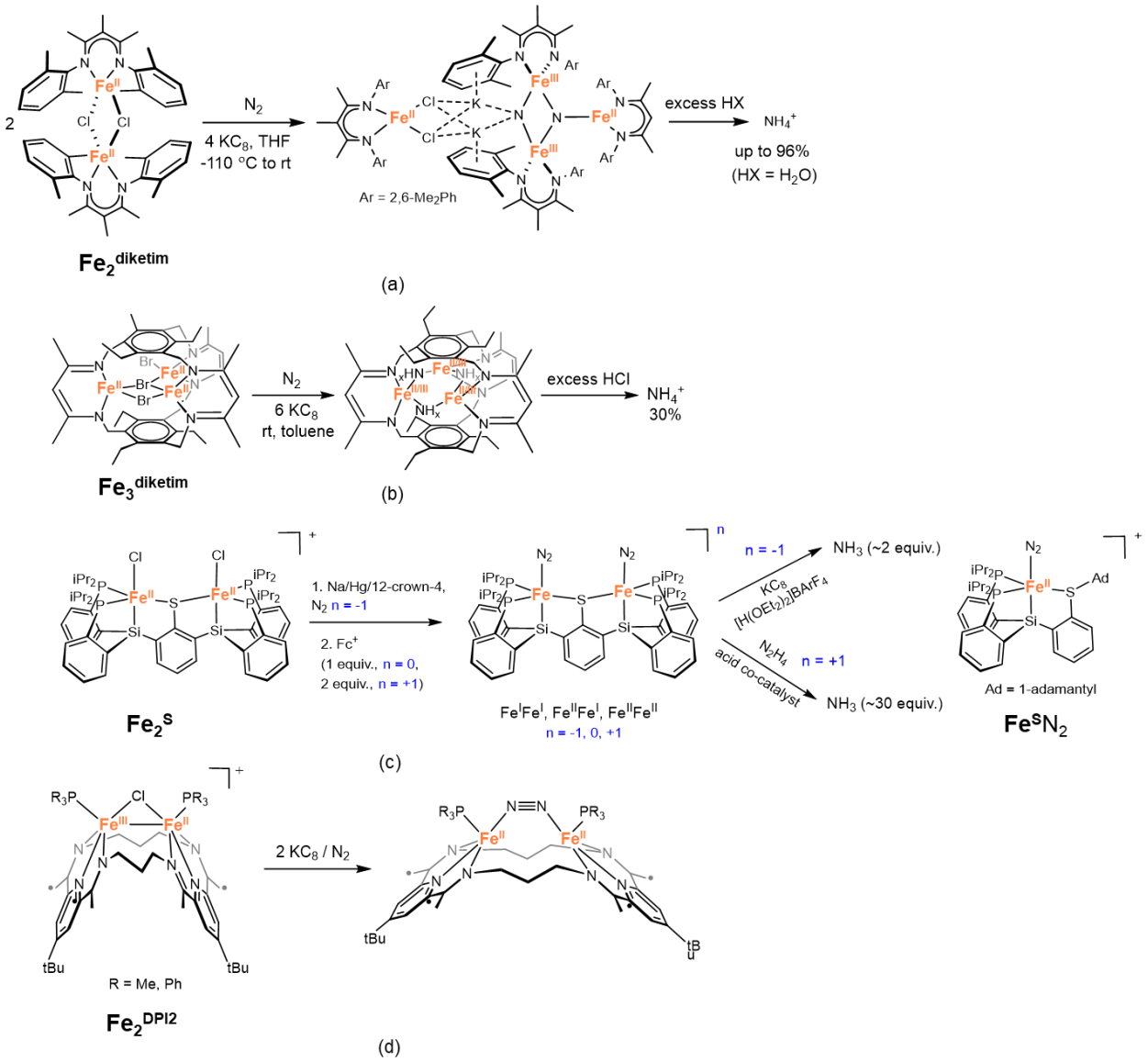

Fig. 13. Reactivity of multiiron complexes with dinitrogen. For comparison with the **Fe_2^S** system, the mononuclear **Fe^SN_2** adduct is also shown.

Very recently, Tomson and co-authors have reported another series of dimetallic iron complexes supported by a binucleating ligand ($[(^3PDI_2)Fe_2(\mu\text{-}Cl)(PR_3)_2]^+$, **$Fe_2^{PDI2}$**, $^3PDI_2$ = pyridine-bis(imine) macrocyclic derivative, R = Me, Ph) Fig. 13d). These compounds have the peculiarity to support non-linear N_2 bridging coordination [184]. Such a constrained geometry (with ~150° Fe-$N_2^{centroid}$-Fe angles) is reminiscent of the bridging side-on coordination of N_2 to iron atoms in the Haber Bosch α-N_2 intermediate (130° Fe-$N_2^{centroid}$-Fe angles) [185, 186], and is also proposed to be involved in N_2 splitting with the above-mentioned Holland complexes [171, 187]. Even if in the Tomson systems the non-linear N_2 coordination mode did not lead to

N_2 cleavage, because of the too strong ligand field donor set, these results pave the way to a promising strategy.

In the context of a multimetallic strategy, the process of dinitrogen reduction to ammonia was made catalytic by Nishibayashi and co-authors, employing a series of binuclear complexes supported by pincer ligands [188-194]. Among them, the dinitrogen-bridged dimolybdenum(0)–dinitrogen complex bearing a tridentate PNP-type pincer ligand $[\{Mo(N_2)_2(^{tBu}PNP)\}_2(\mu\text{-}N_2)]$ (**Mo2**, ^{t}BuPNP = 2,6-bis[(di-*tert*-butylphosphino)methyl]pyridine, Fig. 14) was shown to convert N_2 to NH_3 under ambient conditions upon treatment with cobaltocene ($CoCp_2$) as a reducing agent and 2,6-lutidinium triflate as a proton source. A catalytic mechanism deduced from experimental and theoretical studies is shown in Fig. 14 [195]. It can be separated in three successive phases: (i) protonation of a terminal N_2 ligand (accompanied by ligand exchange on one Mo center, with a triflate that replaces the *trans*-N_2), (ii) the release of the first NH_3 molecule with dissociation of the dinuclear structure, and (iii) the release of the second NH_3 molecule with regeneration of the dinuclear structure. Remarkably, two observations suggest that the dinuclear arrangement is essential for the first protonation step: (i) a mononuclear counterpart of the dinuclear N_2 adduct, $[Mo(N_2)_2(^{tBu}PNP)(PMe_2Ph)]$, is not catalytically active [196]; and (ii) protonation of mononuclear theoretical models $[Mo(N_2)_3(^{tBu}PNP)]$ is predicted to be thermodynamically unlikely [190]. Based on theoretical calculations, the Mo-Mo synergy has been evidenced to be essential, especially for the first protonation, which is the crucial step of the catalytic cycle. Indeed, in **Mo2** the electronic communication between the two Mo centers, mediated by the bridging N_2 ligand, is thought to enable an intermetallic electron transfer from Mo_B to Mo_A, that promotes the protonation of the terminal N_2 ligand on Mo_A.

All these studies show how two or more metal centers offer a unique opportunity to promote N≡N bond splitting. The multimetallic strategy, exploited by nitrogenases and by some synthetic complexes, can assist the process in different ways: (i) multiple metal centers cooperate to form bridging hydrides, used as electron reservoirs to reduce the metal-bound N_2 (FeMo-co); (ii) cooperation between reduced metal centers facilitates multi-electron channelling to N_2 (Holland and Murray complexes); (iii) the synergetic action of alkali cations stabilizes N-adducts (Haber Bosch catalyst, Holland complex); and (iv) electronic communication between metal centers affects the properties and reactivity (e.g. the basicity) of coordinated N_2 (Nishibayashi catalysts). Currently, the major challenge in N_2-reducing synthetic multimetallic systems seems to be the regeneration of the initial complex to make the process catalytic, the unique example of catalysis being achieved with the Nishibayashi's

family of complexes, so far. With this respect, the use of supporting ligands with increased preorganization could help to prevent the collapse of the polynuclear structures that generally follows the protonation of the N-atom bridges.

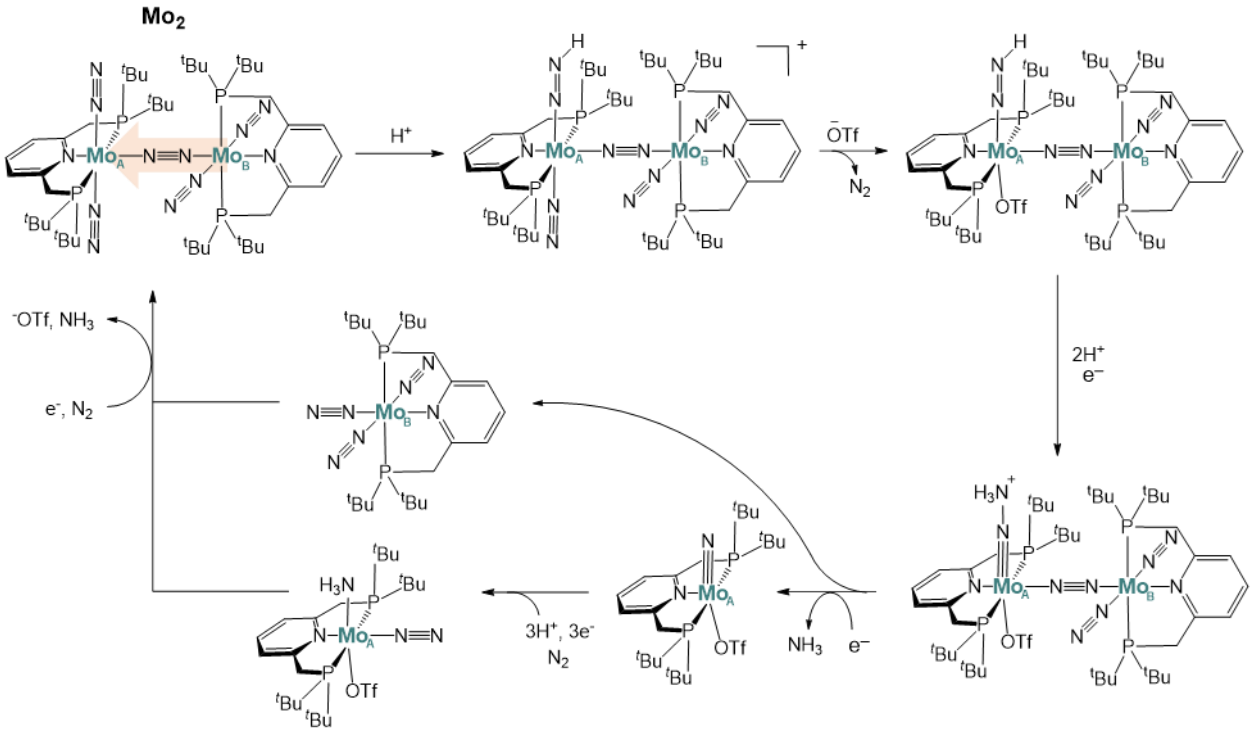

Fig. 14. Mechanism for N_2 reduction to NH_3 catalyzed by the [{Mo(N_2)$_2$(^{tBu}PNP)}$_2$(μ-N_2)] (**Mo$_2$**) complex.

6. Nitrous oxide reduction: from the biological Cu$_Z$ site to multicopper complexes

Nitrous oxide (N_2O) is a potent greenhouse gas, with a 300-fold global warming potential than that of carbon dioxide [197]. Reducing it to benign dinitrogen in a proton-assisted reaction (Equation 6) is thus very attractive.

$$N_2O + 2H^+ + 2e^- \longrightarrow N_2 + H_2O \qquad (6)$$

The inertness of N_2O makes the process kinetically unfavorable [198] and its poor coordination properties (weak σ-donating and π-accepting) make its activation challenging with transition metal ions. However, this last option remains the most common since metal binding typically promotes N-O cleavage and release of N_2 [199].

In nature, nitrous oxide reduction is the last step of the four successive oxygen abstraction reactions occurring in the periplasm of denitrifying bacteria to convert inorganic nitrates into dinitrogen ($NO_3^- \rightarrow NO_2^- \rightarrow NO \rightarrow N_2O \rightarrow N_2$) [200]. For these organisms living in (almost) anoxic environments, this multi-step reduction process corresponds to a form of anaerobic respiration, in which binary nitrogen/oxygen compounds are terminal electron acceptors like dioxygen in aerobic respiration. In denitrifying bacteria, N_2O reduction (Eq. 6) is catalyzed by the nitrous oxide reductase (N_2OR) metalloenzymes [201]. These homo-dimers contain two different copper sites: (i) a unique tetranuclear copper sulfide-bridged "Cu_Z" cluster, bound to the protein backbone via seven histidine residues, which is thought to be the site of N_2O binding and catalytic reduction; (ii) a binuclear Cu_A center delivering electron from biological redox centers (typically *c*-type cytochromes or type I copper proteins) to "Cu_Z".

Two forms of "Cu_Z" (named Cu_Z* and Cu_Z, both isolated and characterized crystallographically, Fig. 15a) coexist in the N_2OR resting state (their relative amount depends on the enzyme purification conditions). The Cu_Z* form (4Cu1S), predominant after aerobic purification, contains a central distorted tetrahedral sulfido ligand μ_4-bridging four copper ions (Cu_I, Cu_{II}, Cu_{III} and Cu_{IV}) in a $Cu^{II}3Cu^{I}$ (one-hole) redox state [202]. Each copper ion is further coordinated by two histidines except Cu_{IV} that is bound to only one, while an additional hydroxo ligand bridges Cu_I and Cu_{IV} along one edge of the cluster. The Cu_Z form (4Cu2S), predominant after anaerobic purification, mainly differs from Cu_Z* by the nature of the ligand that bridges Cu_I and Cu_{IV}, a sulfide instead of a hydroxo, and for the cluster redox state, $2Cu^{II}2Cu^{I}$ [203, 204] (two-hole).

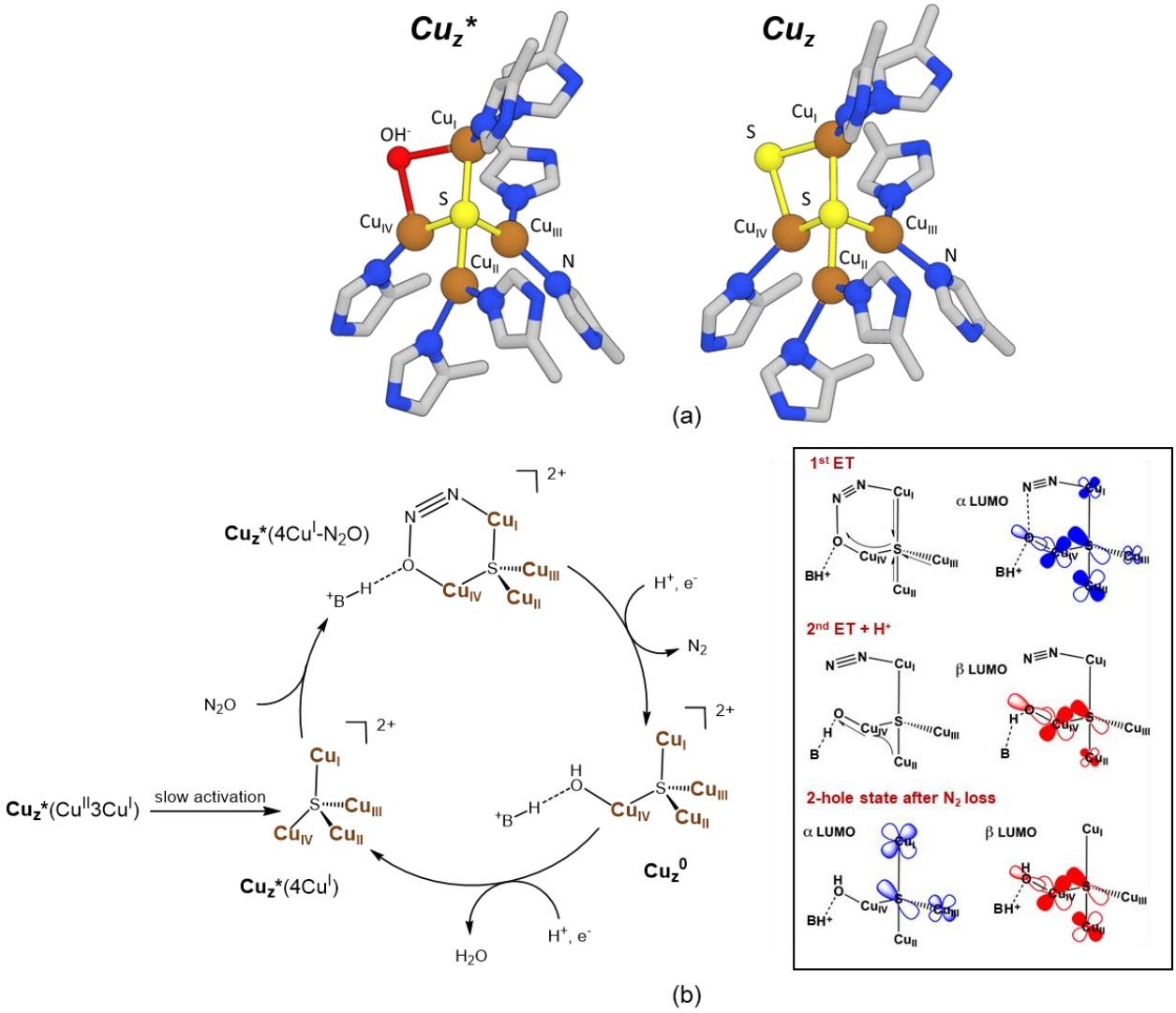

Fig. 15. (a) Structure of the N_2OR active site in the two resting state coexisting forms (*Cu*$_Z$* and *Cu*$_Z$, PDBs 1FWX and 3SBP, respectively); (b) currently accepted catalytic mechanism for biological N_2O reduction (the inset shows a focus on the N_2O binding and N-O cleavage steps, as predicted by DFT, adapted with permission from [205]. Copyright 2017 American Chemical Society; B is a basic site from the protein backbone).

Concerning the N_2OR activity [201, 205-207], the *Cu*$_Z$ form does not seem to be catalytically relevant, since its "active" (reduced) state ($Cu^{II}3Cu^{I}$) reacts too slowly with N_2O [208]. It is thus proposed that *Cu*$_Z$ has a protective role for the enzyme cofactor. Conversely, the *Cu*$_Z$* form is catalytically relevant, even if not directly implicated in catalysis. Indeed, after an activation process (a prolonged incubation in the presence of reduced methyl or benzyl viologen), *Cu*$_Z$* is one-electron reduced to afford the *Cu*$_Z$*($4Cu^{I}$) state that rapidly reduces N_2O into N_2 [209]. The isolated *Cu*$_Z$*($4Cu^{I}$) species is thus proposed to be the first intermediate in the catalytic cycle

(Fig. 15b). Its reaction with N_2O cleaves the N-O bond generating dinitrogen and the so-called Cu_Z^0 intermediate, which has been isolated and spectroscopically characterized [205, 210]. Cu_Z^0 is isoelectronic to Cu_Z* ($Cu^{II}3Cu^{I}$, one-hole state), and structurally similar to it, the only significant difference being the presence of a hydroxo ligand terminally coordinated to Cu_{IV} and stabilized by hydrogen-bonding with the protein backbone, while the OH^- in Cu_Z* was bridging Cu_I and Cu_{IV}. This small structural variation has notable electronic effects and is critical for reactivity: it enables fast one-electron reduction of Cu_Z^0 by the Cu_A center (which is not able to reduce Cu_Z*), regenerating the initial Cu_Z*($4Cu^{I}$) intermediate to complete the cycle [205].

More insights on N_2O binding to Cu_Z*($4Cu^{I}$) and on the following N-O cleavage to afford Cu_Z^0 (i.e. the first step of the catalytic cycle) were provided by DFT calculations performed by Solomon and co-authors [205] (inset of Fig. 15b). Nitrous oxide is first predicted to apically bind to Cu_I in a linear fashion, *via* its terminal N atom. Upon subsequent slight N−O bond elongation, the structure rearranges to form a 139° bent μ-1,3-O,N coordination geometry, with the O atom coordinated to Cu_{IV} and hydrogen-bonded to the protein backbone. The structural attribution for this key intermediate, Cu_Z*($4Cu^{I}$-N_2O), is consistent both (i) with the presence of a terminally bound Cu_{IV}-OH in Cu_Z^0, the O-atom arising from N_2O, and (ii) with the fact that when N_2OR is exposed to the inhibitor iodide, it also bridges the Cu_I and Cu_{IV} ions [211]. The "Cu_Z" electronic structure evolution occurring during N_2O reduction indicates that the two one-electron transfer steps from the {Cu_4S} core to the π* LUMO of N_2O involve all four coppers in a synergetic manner. The first electron is transferred from the cluster *via* Cu_{IV}, but the generated hole (which can be considered as the orbital from which the electron was ejected) is delocalized *via* the μ_4-S^{2-} bridge over the four copper centers. This delocalization lowers the electron transfer energy and results in the cleavage of the N−O bond. The successive proton transfer from the protein backbone to form a terminal Cu_{IV}-OH induces the transfer of a second electron, again *via* Cu_{IV}, with the generated hole being delocalized over Cu_{IV} and Cu_{II}. Following protein backbone reprotonation and N_2 release affords a two-hole intermediate ($2Cu^{II}2Cu^{I}$), with one hole delocalized over Cu_I and Cu_{III} and the second over Cu_{II} and Cu_{IV}. Finally, a last electron transfer from Cu_A generates one-hole Cu_Z^0.

In the proposed N_2OR mechanism, the synergy between the multiple copper ions, structurally and electronically mediated by the μ_4-S^{2-} bridge, is critical for N_2O reductive activation, since: (i) in Cu_Z*($4Cu^{I}$-N_2O), the μ-1,3-O,N bridging mode of N_2O between Cu_I and Cu_{IV} enables its "stabilization" in a bent geometry that promotes back-bonding from copper to the substrate and thus facilitates N−O bond rupture; and (ii) this configuration supports electron delocalization

that lowers the reorganization energy of the redox processes occurring during the catalytic cycle. The need of four cooperating copper centers, even if only two directly interact with N_2O (Cu_I and Cu_{IV}), is confirmed by theoretical calculations [212] and model chemistry [213] predicting that under catalytic conditions a putative dinuclear [$Cu_2(\mu$-S)] core would be deactivated by protonation or oxygenation of the bridging S^{2-} ligand.

In the last decade, inspired by the intriguing structure of "Cu_Z", bioinorganic chemists have developed a series of synthetic multicopper-sulfur models that activate and reduce nitrous oxide. Nevertheless none displays catalytic activity so far [201]. The first functional N_2OR mimic, reported by Tolman and co-authors in 2009, is a mixed-valence tricopper ($Cu^{II}Cu^{I}_2$) cluster bridged by a disulfide moiety, $[(Me_3tacn)_3Cu_3S_2]^{2+}$ (**Cu$_3$**, Me_3tacn = N,N,N-trimethyl-1,4,7-triazacyclonane, Fig. 16) [214]. This complex is able to convert N_2O to N_2 in dichloromethane or tetrahydrofuran solution at low temperature (- 80 °C). Based on both experimental and theoretical data, it was shown that the actual active species is the $[(Me_3tacn)_2Cu^{I}Cu^{II}S_2]^{+}$ complex formed in a dissociative pre-equilibrium. In the predicted reaction mechanism, a μ-1,1-O bridging N_2O transition state is involved (Fig. 16), instead of a bent μ-1,3-O,N N_2O adduct as proposed for "Cu_Z". This intermediate undergoes successive N-O bond scission to form an (undetected) oxo-bridged complex. As in N_2OR, the direct interaction of N_2O with two metal centers seems to facilitate its activation.

Later, Torelli and co-authors reported N_2O reduction activity of a dissymmetric dinuclear copper(I,II) mixed-valence complex containing a {Cu_2S} core and exchangeable positions at the metal sites [215] (**Cu$_2$**, Fig. 16). When bubbling N_2O at room temperature on an acetone solution of the complex, the formation of a hydroxo-bridged dinuclear Cu^{II} adduct was observed concomitantly with release of dinitrogen. Contrarily from the natural and Tolman's systems, N_2O binding does not seem to directly implicate both copper centers. Instead, based on both DFT and experimental data, the authors suggested transient coordination of N_2O to a single copper center, in either a η_1-N or η_1-O mode. However, a Cu–Cu interaction is present in the calculated mixed valence N_2O-bound intermediate, as in the initial complex, so that copper-copper synergy may still play a role in N_2O activation.

With respect to these works, two functional μ_4-sulfido bridged tetracopper clusters reported by Mankad and co-authors replicate more closely the geometry of the "Cu_Z" core. The amidinate-supported [$Cu_4(\mu_4$-S)] model $[(\mu_2\text{-NCN})_4Cu_4(\mu_4\text{-S})]^{-}$ (**Cu$_4$S^N**, NCN^- = $[(2,4,6\text{-}Me_3C_6H_2N)_2CH]^-$, see Fig. 16), in its one-hole state ($Cu^{II}3Cu^{I}$) is capable to stoichiometrically reduce N_2O in tetrahydrofuran at low temperature [216]. As a result, the corresponding one-electron oxidized

cluster (two-holes form, $2Cu^{II}2Cu^{I}$) is generated together with N_2. The authors proposed that one [$Cu_4(\mu_4\text{-}S)$] cluster unit binds and activates the N_2O molecule, while a second cluster molecule acts as a sacrificial reductant, affording the second electron to the substrate.

More recently, the same group described another biomimetic [$Cu_4(\mu_4\text{-}S)$] cluster that is N_2O-reactive in its fully reduced $4Cu^{I}$ state as "Cu_Z", i.e. the $[Cu_4(\mu_4\text{-}S)(\mu_2\text{-dppa})_4]^{2+}$ cluster (**Cu_4S^P**, dppa = $(Ph_2P)_2NH$, see Fig. 16) that contains two NH groups as hydrogen-bond donors in its second coordination sphere [217]. **Cu_4S^P** mediates stoichiometric $2H^+/2e^-$ reduction of N_2O to N_2 and H_2O in the presence of cobaltocene, but only when specific hydrogen bond acceptor solvents (MeOH, acetone) are employed. This behavior is interpreted in terms of a biomimetic hydrogen-bond-induced structural distortion of the cluster that produces a redistribution of the electron density inside the cluster itself (with respect to a non-hydrogen bonded analogue), making favorable N_2O binding and activation at a specific Cu-Cu edge.

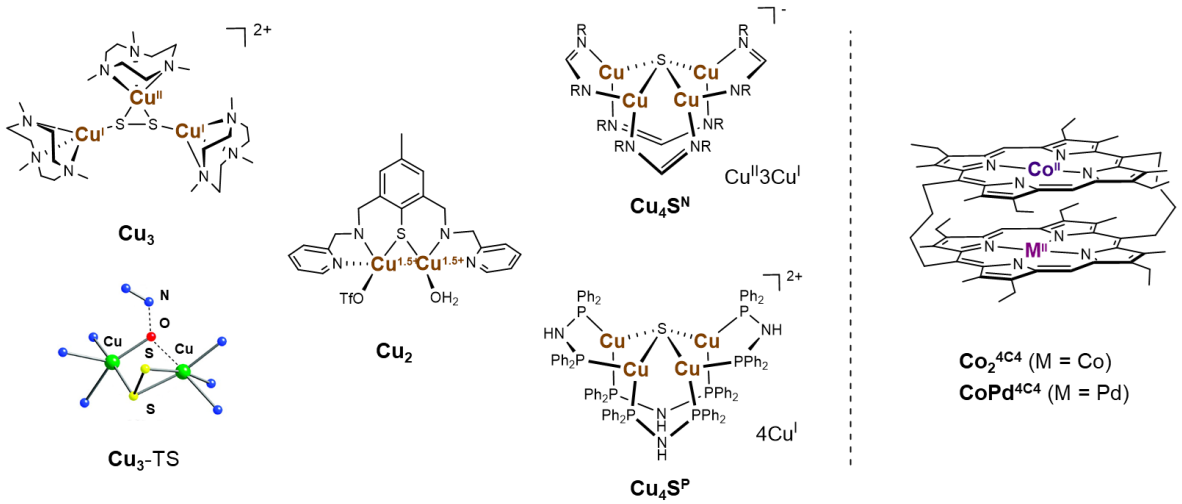

Fig. 16. Multimetallic complexes displaying N_2O reduction reactivity, including both bioinspired multicopper-sulfur "Cu_Z" models (left) and cofacial metal porphyrins (right). In the case of the trinuclear **Cu_3** model, the DFT-calculated dinuclear transition state (**Cu_3-TS**) is also displayed (adapted with permission from [214]. Copyright 2009 American Chemical Society).

Other multimetallic transition metal complexes, not directly inspired from the "Cu_Z" site of N_2O reductase but capable of activating and reducing N_2O electrochemically, have been described by Collman and co-authors, i.e. hydrocarbon-bridged cofacial cobalt porphyrins.[218] More specifically, a greater than thousand-fold enhancement of the N_2O electroreduction rate was observed for the bis-cobalt complex dicobalt(II) bis-2,8,12,18 tetraethyl-3,7,13,17 tetramethyl-5,15 tetramethyleneporphyrin (**Co_2^{4C4}**, Fig. 16) in comparison with the parent heterodinuclear Co^{II}-Pd^{II} derivative (**$CoPd^{4C4}$**, Fig. 16) and with a mononuclear

Co^{II} porphyrin (**Co^{TPP}**, Fig. 7). These results can be explained by the proximity of the two electroactive cobalt centers in **Co_2^{4C4}**, which allows a concerted two-electron N_2O reduction pathway that is not available with **$CoPd^{4C4}$** and **Co^{TPP}**.

Globally, the knowledge extracted from these functional and structural/functional mimics of the "Cu_Z" site of the nitrous oxide reductase strongly supports that a multimetallic center strongly promotes N_2O reduction, since (i) it enables N_2O binding in a bridging mode that is suited for N-O cleavage, and (ii) it facilitates an energetically favorable concerted two-electron N_2O reduction mechanism. Nevertheless, the discovery of a synthetic multicopper center capable of catalyzing N_2O reduction remains a holy grail. To this end, systematic investigations on the aforementioned families of models seem the best viable strategy.

7. Concluding remarks and outlook

In this review, we have discussed multimetallic enzyme active sites together with their respective bio-inspired complexes for which cooperation between metal centers is crucial for small molecule activation. Different types of synergy have been considered, which can be classified in the following categories:

(i) Each metal center activates a different substrate before these react together. This is the case of NiFe- and MoCu-carbon monoxide dehydrogenases, in which one metal (Ni, Cu) binds CO while the second (Fe, Mo) binds H_2O.

(ii) Two or more metal centers are responsible for the activation of a unique substrate in a concerted or sequential way. In nitrous oxide reductase, N_2O is activated simultaneously by two copper centers of its tetranuclear cluster *via* its coordination in a bent μ-1,3-O,N bridging mode that promotes N-O bond cleavage. In a similar way, in the key catalytic intermediates of [NiFe]-hydrogenase, one hydride is bridged between nickel and iron. In Mo-nitrogenase four iron centers are simultaneously involved in the storage of reducing equivalents as bridging hydrides, required to coordinate and activate N_2, and possibly also in channeling electrons to metal-bound N_2 until its complete six-electron reduction. On the other hand, in cytochrome *c* oxidase, both heme iron and copper participate to O_2 activation in a sequential way, with the transient coordination of O_2 to Cu followed by its activation at the heme center, before to act together in the successive O-O cleavage step via the formation of a bridging (hydro)peroxo intermediate.

(iii) One "active" metal binds and activates the substrate, while a second metal "assists" the process (a) by modulating the properties of the entire cofactor, typically its electronic, redox and geometric properties, or (b) by playing a direct role in the redox chemistry of the process. The

first case is that of acetyl-CoA synthase, in which the CO and CH_3^+ substrates bind and react together at Ni_p, whilst Ni_d serves as a regulator. The second case is that of [FeFe]-hydrogenase, in which a terminal hydride is formed at Fe_d, with the Fe_p center that displays only redox activity. We have also described how the investigation of synthetic, bio-inspired multimetallic complexes is crucial (i) to rationalize the role of metal-metal synergy in the corresponding enzymes, and more specifically to understand how this synergy contributes to catalytic performances; and (ii) to exploit these systems, after properly tuning their features accordingly to the previous point, for catalytic applications. Concerning both of these aspects, the use of model complexes allows the definition of structure-activity correlations, including a comparison with the corresponding monometallic systems, the characterization of key intermediates that can be relevant for enzymes, and the exploitation of ligand design as a powerful tool for the optimization of metal-metal cooperation (and consequently of activity) in bio-inspired multimetallic catalysis. There is a growing need for systematic studies to define general trends in multimetallic reactivity. More specifically, the literature lacks studies, in which a common platform, e.g. a dinucleating ligand, is "filled" with various combinations of metal ions, each one playing a specific role, such as the activation of the substrate(s), redox activity, or Lewis acidity. Ideally, such investigation should allow to reach a fine control of the sequence of proton/electron and atom transfer events to the substrate(s) for an optimal catalytic performance.

Acknowledgements

The authors gratefully acknowledge the French National Agency for Research in the framework of the "Investissements d'avenir" program (ANR-15-IDEX-02), ARCANE, "Programme JCJC" (ANR-14-CE06_0002_01), CBH-EUR-GS (ANR-17-EURE-0003) and ANR-DFG (ANR-16-CE92_0012_01).

References

[1] W.B. Tolman, Activation of Small Molecules: Organometallic and Bioinorganic Perspectives, Wiley-VCH Verlag GmbH & Co. KGaA, 2006.
[2] V. Artero, Nat. Energy, 2 (2017) 17131.
[3] J.M. Le, K.L. Bren, ACS Energy Lett., 4 (2019) 2168-2180.
[4] B. Milani, G. Licini, E. Clot, M. Albrecht, Dalton Trans., 45 (2016) 14419-14420.
[5] S.A. Cook, E.A. Hill, A.S. Borovik, Biochemistry, 54 (2015) 4167-4180.
[6] M.W. Ribbe, Metallocofactors that Activate Small Molecules. With Focus on Bioinorganic Chemistry, Springer International Publishing, 2019.

[7] I.G. Powers, C. Uyeda, ACS Catal., 7 (2017) 936-958.
[8] P. Buchwalter, J. Rosé, P. Braunstein, Chem. Rev., 115 (2015) 28-126.
[9] N.P. Mankad, Catalysis with Multinuclear Complexes, in: R.J.M.K. Gebbink, M.E. Moret (Eds.) Non-Noble Metal Catalysis, pp. 49-68.
[10] B. Zhang, L. Sun, Chem. Soc. Rev., 48 (2019) 2216-2264.
[11] W. Lubitz, H. Ogata, O. Rüdiger, E. Reijerse, Chem. Rev., 114 (2014) 4081-4148.
[12] G. Berggren, A. Adamska, C. Lambertz, T.R. Simmons, J. Esselborn, M. Atta, S. Gambarelli, J.M. Mouesca, E. Reijerse, W. Lubitz, T. Happe, V. Artero, M. Fontecave, Nature, 499 (2013) 66-69.
[13] D. Schilter, J.M. Camara, M.T. Huynh, S. Hammes-Schiffer, T.B. Rauchfuss, Chem. Rev., 116 (2016) 8693-8749.
[14] T. Xu, D. Chen, X. Hu, Coord. Chem. Rev., 303 (2015) 32-41.
[15] T.R. Simmons, G. Berggren, M. Bacchi, M. Fontecave, V. Artero, Coord. Chem. Rev., 270-271 (2014) 127-150.
[16] M.E. Ahmed, A. Dey, Curr. Opin. Electrochem., 15 (2019) 155-164.
[17] S. Gao, Y. Liu, Y. Shao, D. Jiang, Q. Duan, Coord. Chem. Rev., 402 (2020) 213081.
[18] U.P. Apfel, F.Y. Pétillon, P. Schollhammer, J. Talarmin, W. Weigand, [FeFe] Hydrogenase Models: an Overview, in: W. Weigand, P. Schollhammer (Eds.) Bioinspired Catalysis, Wiley-VCH Verlag GmbH & Co. KGaA, 2014, pp. 79-104.
[19] J. Dawson, C. Perotto, J. McMaster, M. Schröder, [NiFe] Hydrogenases, in: W. Weigand, P. Schollhammer (Eds.) Bioinspired Catalysis, Wiley-VCH Verlag GmbH & Co. KGaA, 2014, pp. 49-78.
[20] H. Land, M. Senger, G. Berggren, S.T. Stripp, ACS Catal., 10 (2020) 7069-7086.
[21] Y. Nicolet, C. Piras, P. Legrand, C.E. Hatchikian, J.C. Fontecilla-Camps, Structure, 7 (1999) 13-23.
[22] J.W. Peters, W.N. Lanzilotta, B.J. Lemon, L.C. Seefeldt, Science, 282 (1998) 1853-1858.
[23] A. Silakov, B. Wenk, E. Reijerse, W. Lubitz, Phys. Chem. Chem. Phys., 11 (2009) 6592-6599.
[24] J.A. Birrell, V. Pelmenschikov, N. Mishra, H. Wang, Y. Yoda, K. Tamasaku, T.B. Rauchfuss, S.P. Cramer, W. Lubitz, S. DeBeer, J. Am. Chem. Soc., 142 (2020) 222-232.
[25] Y. Nicolet, A.L. de Lacey, X. Vernède, V.M. Fernandez, E.C. Hatchikian, J.C. Fontecilla-Camps, J. Am. Chem. Soc., 123 (2001) 1596-1601.
[26] M.Y. Darensbourg, E.J. Lyon, X. Zhao, I.P. Georgakaki, Proc. Natl. Acad. Sci. U.S.A., 100 (2003) 3683-3688.
[27] S. Rumpel, C. Sommer, E. Reijerse, C. Farès, W. Lubitz, J. Am. Chem. Soc., 140 (2018) 3863-3866.
[28] L.S. Mészáros, P. Ceccaldi, M. Lorenzi, H.J. Redman, E. Pfitzner, J. Heberle, M. Senger, S.T. Stripp, G. Berggren, Chem. Sci., 11 (2020) 4608-4617.
[29] D.W. Mulder, M.W. Ratzloff, M. Bruschi, C. Greco, E. Koonce, J.W. Peters, P.W. King, J. Am. Chem. Soc., 136 (2014) 15394-15402.
[30] M. Haumann, S.T. Stripp, Acc. Chem. Res., 51 (2018) 1755-1763.
[31] P. Rodríguez-Maciá, K. Pawlak, O. Rüdiger, E.J. Reijerse, W. Lubitz, J.A. Birrell, J. Am. Chem. Soc., 139 (2017) 15122-15134.
[32] A. Adamska, A. Silakov, C. Lambertz, O. Rüdiger, T. Happe, E. Reijerse, W. Lubitz, Angew. Chem. Int. Ed., 51 (2012) 11458-11462.
[33] D.W. Mulder, M.W. Ratzloff, E.M. Shepard, A.S. Byer, S.M. Noone, J.W. Peters, J.B. Broderick, P.W. King, J. Am. Chem. Soc., 135 (2013) 6921-6929.
[34] E.J. Reijerse, C.C. Pham, V. Pelmenschikov, R. Gilbert-Wilson, A. Adamska-Venkatesh, J.F. Siebel, L.B. Gee, Y. Yoda, K. Tamasaku, W. Lubitz, T.B. Rauchfuss, S.P. Cramer, J. Am. Chem. Soc., 139 (2017) 4306-4309.

[35] C. Sommer, A. Adamska-Venkatesh, K. Pawlak, J.A. Birrell, O. Rüdiger, E.J. Reijerse, W. Lubitz, J. Am. Chem. Soc., 139 (2017) 1440-1443.
[36] S. Mebs, R. Kositzki, J. Duan, L. Kertess, M. Senger, F. Wittkamp, U.-P. Apfel, T. Happe, S.T. Stripp, M. Winkler, M. Haumann, Biochim. Biophys. Acta, Biophys. Bioenerg., 1859 (2018) 28-41.
[37] H. Ogata, S. Hirota, A. Nakahara, H. Komori, N. Shibata, T. Kato, K. Kano, Y. Higuchi, Structure, 13 (2005) 1635-1642.
[38] A. Volbeda, M.-H. Charon, C. Piras, E.C. Hatchikian, M. Frey, J.C. Fontecilla-Camps, Nature, 373 (1995) 580-587.
[39] M. Brecht, M. van Gastel, T. Buhrke, B. Friedrich, W. Lubitz, J. Am. Chem. Soc., 125 (2003) 13075-13083.
[40] S. Foerster, M. Stein, M. Brecht, H. Ogata, Y. Higuchi, W. Lubitz, J. Am. Chem. Soc., 125 (2003) 83-93.
[41] H. Ogata, K. Nishikawa, W. Lubitz, Nature, 520 (2015) 571-574.
[42] S.J. George, S. Kurkin, R.N.F. Thorneley, S.P.J. Albracht, Biochemistry, 43 (2004) 6808-6819.
[43] R. Hidalgo, P.A. Ash, A.J. Healy, K.A. Vincent, Angew. Chem. Int. Ed., 54 (2015) 7110-7113.
[44] B.J. Murphy, R. Hidalgo, M.M. Roessler, R.M. Evans, P.A. Ash, W.K. Myers, K.A. Vincent, F.A. Armstrong, J. Am. Chem. Soc., 137 (2015) 8484-8489.
[45] B.L. Greene, C.-H. Wu, P.M. McTernan, M.W.W. Adams, R.B. Dyer, J. Am. Chem. Soc., 137 (2015) 4558-4566.
[46] P.A. Ash, S.E.T. Kendall-Price, K.A. Vincent, Acc. Chem. Res., 52 (2019) 3120-3131.
[47] M. Kampa, M.-E. Pandelia, W. Lubitz, M. van Gastel, F. Neese, J. Am. Chem. Soc., 135 (2013) 3915-3925.
[48] C. Tard, C.J. Pickett, Chem. Rev., 109 (2009) 2245-2274.
[49] J.-F. Capon, F. Gloaguen, P. Schollhammer, J. Talarmin, Coord. Chem. Rev., 249 (2005) 1664-1676.
[50] J.-F. Capon, F. Gloaguen, F.Y. Pétillon, P. Schollhammer, J. Talarmin, Coord. Chem. Rev., 253 (2009) 1476-1494.
[51] W. Gao, J. Sun, T. Åkermark, M. Li, L. Eriksson, L. Sun, B. Åkermark, Chem. Eur. J., 16 (2010) 2537-2546.
[52] C. Tard, X. Liu, S.K. Ibrahim, M. Bruschi, L.D. Gioia, S.C. Davies, X. Yang, L.-S. Wang, G. Sawers, C.J. Pickett, Nature, 433 (2005) 610-613.
[53] J.M. Camara, T.B. Rauchfuss, Nat. Chem., 4 (2012) 26-30.
[54] S. Kaur-Ghumaan, M. Stein, Dalton Trans., 43 (2014) 9392-9405.
[55] J.A. Denny, M.Y. Darensbourg, Chem. Rev., 115 (2015) 5248-5273.
[56] S. Ding, P. Ghosh, A.M. Lunsford, N. Wang, N. Bhuvanesh, M.B. Hall, M.Y. Darensbourg, J. Am. Chem. Soc., 138 (2016) 12920-12927.
[57] M.E. Carroll, B.E. Barton, T.B. Rauchfuss, P.J. Carroll, J. Am. Chem. Soc., 134 (2012) 18843-18852.
[58] K. Weber, T. Krämer, H.S. Shafaat, T. Weyhermüller, E. Bill, M. van Gastel, F. Neese, W. Lubitz, J. Am. Chem. Soc., 134 (2012) 20745-20755.
[59] S. Ogo, K. Ichikawa, T. Kishima, T. Matsumoto, H. Nakai, K. Kusaka, T. Ohhara, Science, 339 (2013) 682-684.
[60] B.C. Manor, T.B. Rauchfuss, J. Am. Chem. Soc., 135 (2013) 11895-11900.
[61] D. Brazzolotto, M. Gennari, N. Queyriaux, T.R. Simmons, J. Pécaut, S. Demeshko, F. Meyer, M. Orio, V. Artero, C. Duboc, Nat. Chem., 8 (2016) 1054-1060.
[62] D. Brazzolotto, L. Wang, H. Tang, M. Gennari, N. Queyriaux, C. Philouze, S. Demeshko, F. Meyer, M. Orio, V. Artero, M.B. Hall, C. Duboc, ACS Catal., 8 (2018) 10658-10667.

[63] L. Wang, M. Gennari, A. Barrozo, J. Fize, C. Philouze, S. Demeshko, F. Meyer, M. Orio, V. Artero, C. Duboc, ACS Catal., 10 (2020) 177-186.
[64] M.L. Pegis, C.F. Wise, D.J. Martin, J.M. Mayer, Chem. Rev., 118 (2018) 2340-2391.
[65] M. Wikström, K. Krab, V. Sharma, Chem. Rev., 118 (2018) 2469-2490.
[66] S.B. Adler, Chem. Rev., 104 (2004) 4791-4844.
[67] Z. Gao, L.V. Mogni, E.C. Miller, J.G. Railsback, S.A. Barnett, Energy Environ. Sci., 9 (2016) 1602-1644.
[68] M. Shao, Q. Chang, J.-P. Dodelet, R. Chenitz, Chem. Rev., 116 (2016) 3594-3657.
[69] M.M. Pereira, M. Santana, M. Teixeira, Biochim. Biophys. Acta, Biophys. Bioenerg., 1505 (2001) 185-208.
[70] S. Ferguson-Miller, G.T. Babcock, Chem. Rev., 96 (1996) 2889-2908.
[71] S. Yoshikawa, A. Shimada, Chem. Rev., 115 (2015) 1936-1989.
[72] S.M. Adam, G.B. Wijeratne, P.J. Rogler, D.E. Diaz, D.A. Quist, J.J. Liu, K.D. Karlin, Chem. Rev., 118 (2018) 10840-11022.
[73] S. Nakashima, T. Ogura, T. Kitagawa, Biochim. Biophys. Acta, Biophys. Bioenerg., 1847 (2015) 86-97.
[74] M. Kubo, S. Nakashima, S. Yamaguchi, T. Ogura, M. Mochizuki, J. Kang, M. Tateno, K. Shinzawa-Itoh, K. Kato, S. Yoshikawa, J. Biol. Chem., 288 (2013) 30259-30269.
[75] M.R.A. Blomberg, T. Borowski, F. Himo, R.-Z. Liao, P.E.M. Siegbahn, Chem. Rev., 114 (2014) 3601-3658.
[76] L. Noodleman, W.-G. Han Du, J.A. Fee, A.W. Götz, R.C. Walker, Inorg. Chem., 53 (2014) 6458-6472.
[77] W.-G. Han Du, A.W. Götz, L. Yang, R.C. Walker, L. Noodleman, Phys. Chem. Chem. Phys., 18 (2016) 21162-21171.
[78] A. Bhagi-Damodaran, M.A. Michael, Q. Zhu, J. Reed, B.A. Sandoval, E.N. Mirts, S. Chakraborty, P. Moënne-Loccoz, Y. Zhang, Y. Lu, Nat. Chem., 9 (2017) 257-263.
[79] E. Kim, E.E. Chufan, K. Kamaraj, K.D. Karlin, Chem. Rev., 104 (2004) 1077-1133.
[80] W. Zhang, W. Lai, R. Cao, Chem. Rev., 117 (2017) 3717-3797.
[81] J.P. Collman, P.C. Herrmann, B. Boitrel, X. Zhang, T.A. Eberspacher, L. Fu, J. Wang, D.L. Rousseau, E.R. Williams, J. Am. Chem. Soc., 116 (1994) 9783-9784.
[82] C. Dallacosta, W.A. Alves, A.M. da Costa Ferreira, E. Monzani, L. Casella, Dalton Trans., (2007) 2197-2206.
[83] V. Pirota, F. Gennarini, D. Dondi, E. Monzani, L. Casella, S. Dell'Acqua, New J. Chem., 38 (2014) 518-528.
[84] Z. Halime, H. Kotani, Y. Li, S. Fukuzumi, K.D. Karlin, Proc. Natl. Acad. Sci. U.S.A., 108 (2011) 13990-13994.
[85] H. Shin, D.-H. Lee, C. Kang, K.D. Karlin, Electrochim. Acta, 48 (2003) 4077-4082.
[86] H. Kitagishi, D. Shimoji, T. Ohta, R. Kamiya, Y. Kudo, A. Onoda, T. Hayashi, J. Weiss, J.A. Wytko, K. Kano, Chem. Sci., 9 (2018) 1989-1995.
[87] J.P. Collman, R. Boulatov, C.J. Sunderland, L. Fu, Chem. Rev., 104 (2004) 561-588.
[88] J.P. Collman, N.K. Devaraj, R.A. Decréau, Y. Yang, Y.-L. Yan, W. Ebina, T.A. Eberspacher, C.E.D. Chidsey, Science, 315 (2007) 1565-1568.
[89] S. Chatterjee, K. Sengupta, S. Hematian, K.D. Karlin, A. Dey, J. Am. Chem. Soc., 137 (2015) 12897-12905.
[90] J.P. Collman, M. Rapta, M. Bröring, L. Raptova, R. Schwenninger, B. Boitrel, L. Fu, M. L'Her, J. Am. Chem. Soc., 121 (1999) 1387-1388.
[91] R. Boulatov, J.P. Collman, I.M. Shiryaeva, C.J. Sunderland, J. Am. Chem. Soc., 124 (2002) 11923-11935.
[92] J.P. Collman, C.J. Sunderland, R. Boulatov, Inorg. Chem., 41 (2002) 2282-2291.
[93] J.P. Collman, R. Boulatov, Angew. Chem. Int. Ed., 41 (2002) 3487-3489.

[94] S. Fukuzumi, L. Tahsini, Y.-M. Lee, K. Ohkubo, W. Nam, K.D. Karlin, J. Am. Chem. Soc., 134 (2012) 7025-7035.
[95] L. Tahsini, H. Kotani, Y.-M. Lee, J. Cho, W. Nam, K.D. Karlin, S. Fukuzumi, Chem. Eur. J., 18 (2012) 1084-1093.
[96] C. Liu, H. Lei, Z. Zhang, F. Chen, R. Cao, Chem. Commun., 53 (2017) 3189-3192.
[97] S. Fukuzumi, S. Mandal, K. Mase, K. Ohkubo, H. Park, J. Benet-Buchholz, W. Nam, A. Llobet, J. Am. Chem. Soc., 134 (2012) 9906-9909.
[98] T. Wada, H. Maki, T. Imamoto, H. Yuki, Y. Miyazato, Chem. Commun., 49 (2013) 4394-4396.
[99] M. Gennari, D. Brazzolotto, J. Pecaut, M.V. Cherrier, C.J. Pollock, S. DeBeer, M. Retegan, D.A. Pantazis, F. Neese, M. Rouzieres, R. Clerac, C. Duboc, J. Am. Chem. Soc., 137 (2015) 8644-8653.
[100] L. Wang, M. Gennari, F.G. Cantu Reinhard, J. Gutierrez, A. Morozan, C. Philouze, S. Demeshko, V. Artero, F. Meyer, S.P. de Visser, C. Duboc, J. Am. Chem. Soc., 141 (2019) 8244-8253.
[101] T. Matsumoto, K. Kim, S. Ogo, Angew. Chem. Int. Ed., 50 (2011) 11202-11205.
[102] K. Kim, T. Matsumoto, A. Robertson, H. Nakai, S. Ogo, Chem. Asian J., 7 (2012) 1394-1400.
[103] S. Fukuzumi, K. Okamoto, C.P. Gros, R. Guilard, J. Am. Chem. Soc., 126 (2004) 10441-10449.
[104] A.N. Oldacre, A.E. Friedman, T.R. Cook, J. Am. Chem. Soc., 139 (2017) 1424-1427.
[105] Y. Liu, G. Zhou, Z. Zhang, H. Lei, Z. Yao, J. Li, J. Lin, R. Cao, Chem. Sci., 11 (2020) 87-96.
[106] H. Lei, X. Li, J. Meng, H. Zheng, W. Zhang, R. Cao, ACS Catal., 9 (2019) 4320-4344.
[107] S.W. Ragsdale, M. Kumar, Chem. Rev., 96 (1996) 2515-2540.
[108] M. Can, F.A. Armstrong, S.W. Ragsdale, Chem. Rev., 114 (2014) 4149-4174.
[109] R. Hille, J. Hall, P. Basu, Chem. Rev., 114 (2014) 3963-4038.
[110] H. Dobbek, V. Svetlitchnyi, L. Gremer, R. Huber, O. Meyer, Science, 293 (2001) 1281-1285.
[111] C.L. Drennan, J. Heo, M.D. Sintchak, E. Schreiter, P.W. Ludden, Proc. Natl. Acad. Sci. U. S. A., 98 (2001) 11973-11978.
[112] C. Darnault, A. Volbeda, E.J. Kim, P. Legrand, X. Vernede, P.A. Lindahl, J.C. Fontecilla-Camps, Nat. Struct. Biol., 10 (2003) 271-279.
[113] T.I. Doukov, T.M. Iverson, J. Seravalli, S.W. Ragsdale, C.L. Drennan, Science, 298 (2002) 567-572.
[114] V. Svetlitchnyi, H. Dobbek, W. Meyer-Klaucke, T. Meins, B. Thiele, P. Roemer, R. Huber, O. Meyer, Proc. Natl. Acad. Sci. U. S. A., 101 (2004) 446-451.
[115] R. Burton, M. Can, D. Esckilsen, S. Wiley, S.W. Ragsdale, Chapter Twelve - Production and properties of enzymes that activate and produce carbon monoxide, in: F. Armstrong (Ed.) Methods Enzymol., Academic Press, 2018, pp. 297-324.
[116] H. Dobbek, L. Gremer, R. Kiefersauer, R. Huber, O. Meyer, Proc. Natl. Acad. Sci. U. S. A., 99 (2002) 15971-15976.
[117] M. Gnida, R. Ferner, L. Gremer, O. Meyer, W. Meyer-Klaucke, Biochemistry, 42 (2003) 222-230.
[118] D. Ghosh, S. Sinhababu, B.D. Santarsiero, N.P. Mankad, J. Am. Chem. Soc., 142 (2020) 12635-12642.
[119] C. Yoo, Y. Lee, Chem. Sci., 8 (2017) 600-605.
[120] S. Ogo, Y. Mori, T. Ando, T. Matsumoto, T. Yatabe, K.-S. Yoon, H. Hayashi, M. Asano, Angew. Chem., Int. Ed., 56 (2017) 9723-9726.

[121] C. Gourlay, D.J. Nielsen, J.M. White, S.Z. Knottenbelt, M.L. Kirk, C.G. Young, J. Am. Chem. Soc., 128 (2006) 2164-2165.
[122] S. Groysman, A. Majumdar, S.-L. Zheng, R.H. Holm, Inorg. Chem., 49 (2010) 1082-1089.
[123] M. Takuma, Y. Ohki, K. Tatsumi, Inorg. Chem., 44 (2005) 6034-6043.
[124] C. Gourlay, D.J. Nielsen, D.J. Evans, J.M. White, C.G. Young, Chem. Sci., 9 (2018) 876-888.
[125] T.S. Hollingsworth, R.L. Hollingsworth, R.L. Lord, S. Groysman, Dalton Trans., 47 (2018) 10017-10024.
[126] P. Zimmermann, C. Limberg, J. Am. Chem. Soc., 139 (2017) 4233-4242.
[127] C. Yoo, S. Oh, J. Kim, Y. Lee, Chem. Sci., 5 (2014) 3853-3858.
[128] D. Sahoo, C. Yoo, Y. Lee, J. Am. Chem. Soc., 140 (2018) 2179-2185.
[129] A.C. Manesis, B.W. Musselman, B.C. Keegan, J. Shearer, N. Lehnert, H.S. Shafaat, Inorg. Chem., 58 (2019) 8969-8982.
[130] M. Ito, M. Kotera, T. Matsumoto, K. Tatsumi, Proc. Natl. Acad. Sci. U.S.A., 106 (2009) 11862-11866.
[131] T. Matsumoto, M. Ito, M. Kotera, K. Tatsumi, Dalton Trans., 39 (2010) 2995-2997.
[132] J.N. Galloway, A.R. Townsend, J.W. Erisman, M. Bekunda, Z. Cai, J.R. Freney, L.A. Martinelli, S.P. Seitzinger, M.A. Sutton, Science, 320 (2008) 889-892.
[133] A. Grinberg Dana, O. Elishav, A. Bardow, G.E. Shter, G.S. Grader, Angew. Chem. Int. Ed., 55 (2016) 8798-8805.
[134] T. Kandemir, M.E. Schuster, A. Senyshyn, M. Behrens, R. Schlögl, Angew. Chem. Int. Ed., 52 (2013) 12723-12726.
[135] B.M. Hoffman, D. Lukoyanov, Z.-Y. Yang, D.R. Dean, L.C. Seefeldt, Chem. Rev., 114 (2014) 4041-4062.
[136] O. Einsle, D.C. Rees, Chem. Rev., 120 (2020) 4969-5004.
[137] C. Van Stappen, L. Decamps, G.E. Cutsail, R. Bjornsson, J.T. Henthorn, J.A. Birrell, S. DeBeer, Chem. Rev., (2020) 5005–5081.
[138] L.C. Seefeldt, Z.-Y. Yang, D.A. Lukoyanov, D.F. Harris, D.R. Dean, S. Raugei, B.M. Hoffman, Chem. Rev., 120 (2020) 5082-5106.
[139] H.L. Rutledge, F.A. Tezcan, Chem. Rev., 120 (2020) 5158-5193.
[140] T. Spatzal, M. Aksoyoglu, L. Zhang, S.L.A. Andrade, E. Schleicher, S. Weber, D.C. Rees, O. Einsle, Science, 334 (2011) 940-940.
[141] D. Lukoyanov, Z.-Y. Yang, D.R. Dean, L.C. Seefeldt, B.M. Hoffman, J. Am. Chem. Soc., 132 (2010) 2526-2527.
[142] H.-P. Jia, E.A. Quadrelli, Chem. Soc. Rev., 43 (2014) 547-564.
[143] D.J. Lowe, R.N. Thorneley, Biochem. J, 224 (1984) 877-886.
[144] R.N.F. Thorneley, D.J. Lowe, Biochem. J, 224 (1984) 887-894.
[145] B.M. Hoffman, D.R. Dean, L.C. Seefeldt, Acc. Chem. Res., 42 (2009) 609-619.
[146] B.M. Hoffman, D. Lukoyanov, D.R. Dean, L.C. Seefeldt, Acc. Chem. Res., 46 (2013) 587-595.
[147] D. Lukoyanov, Z.-Y. Yang, B.M. Barney, D.R. Dean, L.C. Seefeldt, B.M. Hoffman, Proc. Natl. Acad. Sci. U.S.A., 109 (2012) 5583-5587.
[148] D. Lukoyanov, N. Khadka, Z.-Y. Yang, D.R. Dean, L.C. Seefeldt, B.M. Hoffman, J. Am. Chem. Soc., 138 (2016) 10674-10683.
[149] V. Hoeke, L. Tociu, D.A. Case, L.C. Seefeldt, S. Raugei, B.M. Hoffman, J. Am. Chem. Soc., 141 (2019) 11984-11996.
[150] R.Y. Igarashi, M. Laryukhin, P.C. Dos Santos, H.-I. Lee, D.R. Dean, L.C. Seefeldt, B.M. Hoffman, J. Am. Chem. Soc., 127 (2005) 6231-6241.

[151] D. Lukoyanov, Z.-Y. Yang, N. Khadka, D.R. Dean, L.C. Seefeldt, B.M. Hoffman, J. Am. Chem. Soc., 137 (2015) 3610-3615.
[152] Z.-Y. Yang, N. Khadka, D. Lukoyanov, B.M. Hoffman, D.R. Dean, L.C. Seefeldt, Proc. Natl. Acad. Sci. U. S. A., 110 (2013) 16327-16332.
[153] B.M. Barney, J. McClead, D. Lukoyanov, M. Laryukhin, T.-C. Yang, D.R. Dean, B.M. Hoffman, L.C. Seefeldt, Biochemistry, 46 (2007) 6784-6794.
[154] L.C. Seefeldt, B.M. Hoffman, D.R. Dean, Annu. Rev. Biochem, 78 (2009) 701-722.
[155] B.M. Barney, J. McClead, D. Lukoyanov, M. Laryukhin, T.-C. Yang, D.R. Dean, B.M. Hoffman, L.C. Seefeldt, Biochemistry, 46 (2007) 6784-6794.
[156] B.M. Barney, M. Laryukhin, R.Y. Igarashi, H.-I. Lee, P.C. Dos Santos, T.-C. Yang, B.M. Hoffman, D.R. Dean, L.C. Seefeldt, Biochemistry, 44 (2005) 8030-8037.
[157] B.M. Barney, T.-C. Yang, R.Y. Igarashi, P.C. Dos Santos, M. Laryukhin, H.-I. Lee, B.M. Hoffman, D.R. Dean, L.C. Seefeldt, J. Am. Chem. Soc., 127 (2005) 14960-14961.
[158] R. Bjornsson, F.A. Lima, T. Spatzal, T. Weyhermueller, P. Glatzel, E. Bill, O. Einsle, F. Neese, S. DeBeer, Chem. Sci., 5 (2014) 3096-3103.
[159] A.L. Nagelski, M.S. Fataftah, M.M. Bollmeyer, S.F. McWilliams, S.N. MacMillan, B.Q. Mercado, K.M. Lancaster, P.L. Holland, Chem. Sci., (2020), ahead of print.
[160] Y. Roux, C. Duboc, M. Gennari, ChemPhysChem, 18 (2017) 2606-2617.
[161] M.J. Chalkley, M.W. Drover, J.C. Peters, Chem. Rev., 120 (2020) 5582-5636.
[162] D. Singh, W.R. Buratto, J.F. Torres, L.J. Murray, Chem. Rev., 120 (2020) 5517-5581.
[163] K. Tanifuji, Y. Ohki, Chem. Rev., 120 (2020) 5194-5251.
[164] D.E. DeRosha, P.L. Holland, Proc. Natl. Acad. Sci. U.S.A., 115 (2018) 5054-5056.
[165] I. Čorić, P.L. Holland, J. Am. Chem. Soc., 138 (2016) 7200-7211.
[166] M.M. Rodriguez, E. Bill, W.W. Brennessel, P.L. Holland, Science, 334 (2011) 780-783.
[167] G.P. Connor, P.L. Holland, Catal. Today, 286 (2017) 21-40.
[168] K.P. Chiang, S.M. Bellows, W.W. Brennessel, P.L. Holland, Chem. Sci., 5 (2014) 267-274.
[169] K.C. Macleod, P.L. Holland, Nat. Chem., 5 (2013) 559-565.
[170] K.C. MacLeod, D.J. Vinyard, P.L. Holland, J. Am. Chem. Soc., 136 (2014) 10226-10229.
[171] K. Grubel, W.W. Brennessel, B.Q. Mercado, P.L. Holland, J. Am. Chem. Soc., 136 (2014) 16807-16816.
[172] K.C. MacLeod, S.F. McWilliams, B.Q. Mercado, P.L. Holland, Chem. Sci., 7 (2016) 5736-5746.
[173] S.F. McWilliams, P.L. Holland, Acc. Chem. Res., 48 (2015) 2059-2065.
[174] M.G. Scheibel, S. Schneider, Angew. Chem. Int. Ed., 51 (2012) 4529-4531.
[175] Y. Lee, F.T. Sloane, G. Blondin, K.A. Abboud, R. García-Serres, L.J. Murray, Angew. Chem. Int. Ed., 54 (2015) 1499-1503.
[176] S.E. Creutz, J.C. Peters, J. Am. Chem. Soc., 137 (2015) 7310-7313.
[177] S.C. Lee, R.H. Holm, Proc. Natl. Acad. Sci. U.S.A., 100 (2003) 3595-3600.
[178] Y. Ohki, Y. Ikagawa, K. Tatsumi, J. Am. Chem. Soc., 129 (2007) 10457-10465.
[179] Y. Zhang, J.-L. Zuo, H.-C. Zhou, R.H. Holm, J. Am. Chem. Soc., 124 (2002) 14292-14293.
[180] S. Ohta, Y. Ohki, T. Hashimoto, R.E. Cramer, K. Tatsumi, Inorg. Chem., 51 (2012) 11217-11219.
[181] S.C. Lee, W. Lo, R.H. Holm, Chem. Rev., 114 (2014) 3579-3600.
[182] K. Tanifuji, C.C. Lee, Y. Ohki, K. Tatsumi, Y. Hu, M.W. Ribbe, Angew. Chem. Int. Ed., 54 (2015) 14022-14025.
[183] A. Takaoka, N.P. Mankad, J.C. Peters, J. Am. Chem. Soc., 133 (2011) 8440-8443.
[184] T. Liu, M.R. Gau, N.C. Tomson, J. Am. Chem. Soc., 142 (2020) 8142-8146.
[185] F. Bozso, G. Ertl, M. Grunze, M. Weiss, J. Catal., 49 (1977) 18-41.

[186] J. Qian, Q. An, A. Fortunelli, R.J. Nielsen, W.A. Goddard, J. Am. Chem. Soc., 140 (2018) 6288-6297.
[187] T.M. Figg, P.L. Holland, T.R. Cundari, Inorg. Chem., 51 (2012) 7546-7550.
[188] K. Arashiba, Y. Miyake, Y. Nishibayashi, Nat. Chem., 3 (2011) 120-125.
[189] A. Eizawa, K. Arashiba, H. Tanaka, S. Kuriyama, Y. Matsuo, K. Nakajima, K. Yoshizawa, Y. Nishibayashi, Nat. Commun., 8 (2017) 14874.
[190] H. Tanaka, K. Arashiba, S. Kuriyama, A. Sasada, K. Nakajima, K. Yoshizawa, Y. Nishibayashi, Nat. Commun., 5 (2014) 3737.
[191] E. Kinoshita, K. Arashiba, S. Kuriyama, Y. Miyake, R. Shimazaki, H. Nakanishi, Y. Nishibayashi, Organometallics, 31 (2012) 8437-8443.
[192] S. Kuriyama, K. Arashiba, K. Nakajima, H. Tanaka, N. Kamaru, K. Yoshizawa, Y. Nishibayashi, J. Am. Chem. Soc., 136 (2014) 9719-9731.
[193] S. Kuriyama, K. Arashiba, K. Nakajima, H. Tanaka, K. Yoshizawa, Y. Nishibayashi, Chem. Sci., 6 (2015) 3940-3951.
[194] Y. Tanabe, Y. Sekiguchi, H. Tanaka, A. Konomi, K. Yoshizawa, S. Kuriyama, Y. Nishibayashi, Chem. Commun., (2020).
[195] H. Tanaka, Y. Nishibayashi, K. Yoshizawa, Acc. Chem. Res., 49 (2016) 987-995.
[196] K. Arashiba, K. Sasaki, S. Kuriyama, Y. Miyake, H. Nakanishi, Y. Nishibayashi, Organometallics, 31 (2012) 2035-2041.
[197] A.R. Ravishankara, J.S. Daniel, R.W. Portmann, Science, 326 (2009
) 123-125.
[198] W.C. Trogler, Coord. Chem. Rev., 187 (1999) 303-327.
[199] W.B. Tolman, Angew. Chem. Int. Ed., 49 (2010) 1018-1024.
[200] W.G. Zumft, Microbiol. Mol. Biol. Rev., 61 (1997) 533-616.
[201] S.R. Pauleta, M.S.P. Carepo, I. Moura, Coord. Chem. Rev., 387 (2019) 436-449.
[202] T. Haltia, K. Brown, M. Tegoni, C. Cambillau, M. Saraste, K. Mattila, K. Djinovic-Carugo, Biochem. J, 369 (2003) 77-88.
[203] A. Pomowski, W.G. Zumft, P.M.H. Kroneck, O. Einsle, Nature, 477 (2011) 234-237.
[204] A. Wuest, L. Schneider, A. Pomowski, W.G. Zumft, P.M.H. Kroneck, O. Einsle, Biol. Chem., 393 (2012) 1067-1077.
[205] E.M. Johnston, C. Carreira, S. Dell'Acqua, S.G. Dey, S.R. Pauleta, I. Moura, E.I. Solomon, J. Am. Chem. Soc., 139 (2017) 4462-4476.
[206] C. Carreira, S.R. Pauleta, I. Moura, J. Inorg. Biochem., 177 (2017) 423-434.
[207] S.R. Pauleta, S. Dell'Acqua, I. Moura, Coord. Chem. Rev., 257 (2013) 332-349.
[208] E.M. Johnston, S. Dell'Acqua, S. Ramos, S.R. Pauleta, I. Moura, E.I. Solomon, J. Am. Chem. Soc., 136 (2014) 614-617.
[209] S. Ghosh, S.I. Gorelsky, P. Chen, I. Cabrito, Moura, I. MouraMoura, E.I. Solomon, J. Am. Chem. Soc., 125 (2003) 15708-15709.
[210] S. Dell'Acqua, S.R. Pauleta, P.M. Paes de Sousa, E. Monzani, L. Casella, J.J.G. Moura, I. Moura, J. Biol. Inorg. Chem., 15 (2010) 967-976.
[211] K. Paraskevopoulos, S.V. Antonyuk, R.G. Sawers, R.R. Eady, S.S. Hasnain, J. Mol. Biol., 362 (2006) 55-65.
[212] S.I. Gorelsky, S. Ghosh, E.I. Solomon, J. Am. Chem. Soc., 128 (2006) 278-290.
[213] S. Bagherzadeh, N.P. Mankad, Chem. Commun., 54 (2018) 1097-1100.
[214] I. Bar-Nahum, A.K. Gupta, S.M. Huber, M.Z. Ertem, C.J. Cramer, W.B. Tolman, J. Am. Chem. Soc., 131 (2009) 2812-2814.
[215] C. Esmieu, M. Orio, S. Torelli, L. Le Pape, J. Pécaut, C. Lebrun, S. Ménage, Chem. Sci., 5 (2014) 4774-4784.
[216] B.J. Johnson, W.E. Antholine, S.V. Lindeman, M.J. Graham, N.P. Mankad, J. Am. Chem. Soc., 138 (2016) 13107-13110.

[217] C.-W. Hsu, S.C. Rathnayaka, S.M. Islam, S.N. MacMillan, N.P. Mankad, Angew. Chem. Int. Ed., 59 (2020) 627-631.
[218] J.P. Collman, M. Marrocco, C.M. Elliott, M. L'Her, J. Electroanal. Chem. Interfacial Electrochem., 124 (1981) 113-131.